2003

An Information Theoretic Study of the Ising Antiferromagnet with Quenched Dilution on a Triangular Lattice

Matthew D. Robinson

AN INFORMATION THEORETIC STUDY OF THE ISING ANTIFERROMAGNET WITH QUENCHED DILUTION ON A TRIANGULAR LATTICE

By

Matthew D. Robinson

B.S. University of Nevada, Reno, 1999

B.A. University of Nevada, Reno, 1999

A THESIS

Submitted in Partial Fulfillment of the

Requirements for the Degree of

Master of Science

(in Physics)

The Graduate School

The University of Maine

August, 2003

Advisory Committee:

Susan R. McKay, Professor of Physics, Co-Advisor

David P. Feldman, Professor of Physics and Mathematics, College of the Atlantic, Co-Advisor

Charles W. Smith, Professor of Physics

AN INFORMATION THEORETIC STUDY OF THE ISING ANTIFERROMAGNET WITH QUENCHED DILUTION ON A TRIANGULAR LATTICE

By Matthew D. Robinson

Thesis Co-Advisors: Dr. Susan R. McKay, Dr. David P. Feldman

An Abstract of the Thesis Presented
in Partial Fulfillment of the Requirements for the
Degree of Master of Science
(in Physics)
August, 2003

This investigation applies information theoretic techniques to study the ordering and structure of the Ising antiferromagnet with quenched disorder on a triangular lattice. The pure system shows no phase transition due to the high degree of frustration present. However, when quenched vacancies are introduced randomly into this geometrically frustrated system, a phase transition at finite temperature, to an ordered phase, can arise. If the vacancies are introduced on all three sublattices of the triangular lattice, then a two-dimensional spin-glass transition occurs. If dilution takes place on only one sublattice, then the other two sublattices develop magnetizations below the critical temperature. These magnetizations are equal in magnitude but opposite in sign, producing a system that still exhibits no net magnetization. The diluted sublattice exhibits spin-glass ordering, but no net magnetization.

Thus, this model exhibits two generic features that merit detailed study: a two-dimensional spin-glass transition and "order arising from disorder", in this case the

introduction of randomly placed vacancies. To investigate these transitions and the ordering that occurs, we have used both traditional quantities from statistical mechanics, such as the sublattice magnetizations, the Edwards-Anderson order parameter, and the specific heat. In addition, we have calculated the Shannon entropy and the excess entropy, two quantities from the field of information theory which are frequently used to characterize the structure and complexity of dynamical systems.

This study is the first to apply this type of Shannon entropy calculation to a two-dimensional system with quenched randomness, so an initial part of our investigation included verifying that the Shannon entropy calculated this way in fact equals the thermodynamic entropy of the system. The Shannon entropy results show excellent agreement with entropies obtained by integrating the specific heat divided by the temperature. Our work is also the first study, to our knowledge, to use this approach for a triangular lattice and for a case in which individual members of the ensemble are not translationally invariant, although the ensemble as a whole does possess translational invariance. Thus we have established the broader applicability of this approach.

The method that we have introduced to treat non-translationally invariant systems employs a set of shapes planted within the lattice. We calculate the entropy and excess entropy contributions of each shape and then average them to obtain the lattice properties. This procedure yields a spatial map of local properties. The distribution of these local properties provides a new way to characterize order in complex lattice systems. In the triangular antiferromagnet with quenched dilution, the distribution of local entropies shows a dramatic broadening at low temperatures, indicating that the total entropy of the system is not shared evenly across the lattice. The entropy contributions from some regions exhibit local reentrance as a function of temperature, even though the total entropy of the system decreases monotonically during cooling.

DEDICATION

To my wife, Kate – without whom it would not have been possible.

ACKNOWLEDGEMENTS

I would like to express my sincere appreciation to my co-advisors Susan McKay and David Feldman, without their continuous advice, assistance, and constant encouragement this work would not have been possible. Susan, thank you for tolerating many, many interruptions first, while I was debugging my code and later, while I was writing this thesis. I cannot express my appreciation for your patience. Dave, thank you for being so prompt in critiquing the seemingly infinite number of revisions this thesis has gone through. You lightened my load more than you can know.

My special thanks also goes to Charles W. Smith for his academic suggestions and willingness to serve on my graduate committee.

Further, I would like to thank Ivan Georgiev for helping me eschew the obfuscation associated with using information theory to quantify physical phenomena. I would like to thank all the physics and astronomy graduate students of The University of Maine, especially Jim, Vaithee, Simon, Vince, Ross, and Debbie, for their technical and emotional support.

Finally I want to thank Eric Wages and the Blackbear cluster, which made the large scale data acquisition of this thesis possible.

TABLE OF CONTENTS

LIST OF FIGURES

CHAPTER 1

INTRODUCTION

This investigation applies information theoretic techniques in a new way to study the ordering and structure of the Ising antiferromagnet with quenched disorder on a triangular lattice. The pure system shows no phase transition due to the high degree of frustration present. In a frustrated system such as this one, there is no spin configuration that minimizes the energy of each bond and the ground state is typically degenerate. When quenched vacancies are introduced randomly into this geometrically frustrated system, a phase transition occurs at finite temperature to an ordered phase. If vacancies are introduced on all three sublattices of the triangular lattice, then a two-dimensional spin-glass transition occurs. If dilution takes place on only one sublattice, then the other two sublattices develop magnetizations below the critical temperature. These magnetizations are equal in magnitude but opposite in sign, producing a system that still exhibits no net magnetization. The diluted sublattice exhibits spin-glass ordering, but no net magnetization.

Thus, this model exhibits two generic features that merit detailed study: a two-dimensional spin-glass transition and "order arising from disorder", with the disorder, in this case, created via the introduction of randomly placed vacancies. These vacancies are an example of quenched randomness since, once positioned, they remain immobile as the system undergoes thermal fluctuations. To investigate these transitions and the ordering that occurs, we have used traditional quantities from statistical mechanics, such as the sublattice magnetization, the Edwards-Anderson order parameter, and the specific heat. In addition, we have calculated the Shannon entropy and the excess entropy, two quantities from the field of information theory

which are frequently used to characterize the structure and complexity of dynamical systems.

Fully characterizing the nature of the ordering that occurs in models of disordered magnetic systems, such as this one, has been a long-standing challenge in statistical physics. The onset of spin-glass ordering is usually associated with broken ergodicity, where the phase space of the system is divided into several (or perhaps many) distinct regions with boundaries across which the system cannot pass with finite probability in the thermodynamic limit. Unlike non-glassy transitions, it is generally believed that these regions of phase space are not related by any simple symmetry operation, such as a global spin flip or a global spin rotation.

This study is the first to apply this type of Shannon entropy calculation to a two-dimensional system with quenched randomness, so an initial part of our investigation included verifying that the Shannon entropy calculated this way in fact equals the thermodynamic entropy of the system. The Shannon entropy results show excellent agreement with entropies obtained by integrating the specific heat divided by the temperature. Our work is also the first study, to our knowledge, to use this approach for a triangular lattice and for a case in which individual members of the ensemble are not translationally invariant, although the ensemble as a whole does possess translational invariance. Thus we have established, through this study, the broader applicability of this approach.

The method that we have introduced to treat non-translationally invariant systems employs a set of shapes planted within the lattice. We calculate the entropy and excess entropy contributions of each shape and then average them to obtain the lattice properties. This procedure yields a spatial map of local properties. The distribution of these local properties provides a new way to characterize order in complex lattice systems.

In the triangular antiferromagnet with quenched dilution, the distribution of local entropies shows a dramatic broadening at low temperatures, indicating that the total entropy of the system is not shared evenly across the lattice. The entropy contributions from some regions exhibit local reentrance as a function of temperature, even though the total entropy of the system decreases monotonically during cooling as expected. The information theoretic method provides spatial maps indicating high and low entropy and excess entropy regions as this ordering occurs. Thus, this approach provides a new way to quantify and visualize spin-glass ordering, all within a two-dimensional system.

This thesis is organized as follows. Chapter 2 briefly reviews the model that we have studied and its known properties. Chapters 3 and 4 present the relevant background information about statistical mechanics and our methods respectively. We then present our results in Chapter 5 and conclude in Chapter 6 by providing a summary of the main findings and suggestions of several areas for future investigation.

CHAPTER 2

THE MODEL

2.1 The Ising antiferromagnet on a triangular lattice

This thesis investigates the Ising antiferromagnet on a two-dimensional triangular lattice. Each site on the lattice has a spin whose dipole moment points either out of the lattice plane or into it. Each spin interacts with its six nearest neighbors with interaction energy J and applied external magnetic field H. The Hamiltonian for this system is

$$\mathcal{H} = -J \sum_{\langle ij \rangle} \sigma_i \sigma_j - H \sum_i \sigma_i, \tag{1}$$

where $\sum_{\langle ij \rangle}$ means that the summation is over nearest neighbors. Each spin σ_i is a binary variable: $\sigma_i \in \{-1, +1\}$. The negative sign before the first term, the interaction term, lowers the energy when its nearest neighbors are aligned for positive coupling constant J (ferromagnetic bonds), and favors antiparallel alignment for negative J (antiferromagnetic bonds). In the following, we fix $J = -1$. Thus, neighboring pairs of spins in an antiferromagnetic arrangement are energetically favored.

The unit cell of the triangular lattice is a rhombus which can be thought of as two equilateral triangles, or *plaquettes*. For the case of antiferromagnetic bonds, the plaquettes are *geometrically frustrated*, and at least one of the three bonds must contribute positively to the energy. As this is the case for every plaquette, the antiferromagnet on the triangular lattice is maximally frustrated. In frustrated systems multiple deep wells occur in the graph of the free energy as a function of order parameter (magnetization, etc.), leading to what is known as a *rugged free energy landscape.*

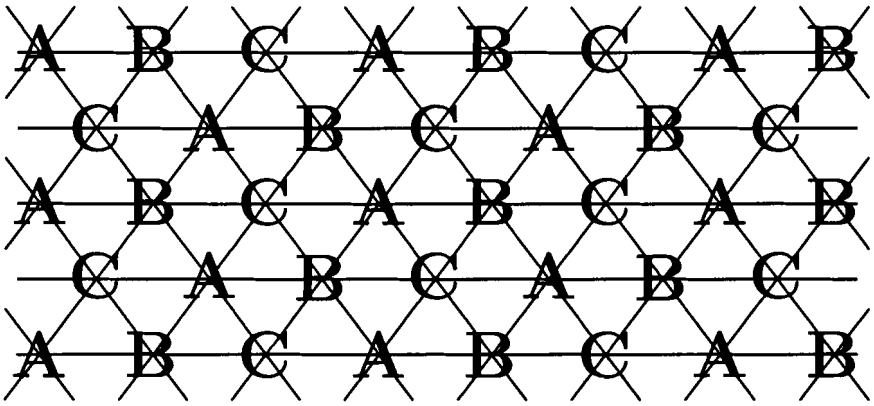

Figure 1: A triangular lattice with the three sublattices denoted by the letters A, B and C. A spin on one sublattice has no nearest neighbor on the same sublattice.

The pure Ising antiferromagnet on a triangular lattice does not order at finite temperature, and there is a large degeneracy of the ground state. The entropy due to the zero-temperature degeneracy, the *residual entropy* $s(0)$, is known exactly from transfer-matrix calculations to be $0.323066\,k_B$ (Wannier, 1950), where k_B is Boltzmann's constant.

2.2 Dilution

The introduction of *quenched vacancies* (i.e. fixed, unoccupied sites in the lattice) relieves the frustration and causes a phase transition to occur (Grest and Gabl, 1979). Grest and Gabl studied this model by randomly deleting sites over the whole lattice. They obtained Monte Carlo results showing that the antiferromagnet exhibits long-range, spin-glass ordering if quenched vacancies are introduced randomly. Specifically, Grest and Gabl report that nonvanishing quenched dilution gives rise to a second order phase transition. As quenched dilution is increased to 50%, the lattice reaches the *percolation threshold*, the point at which so many sites are missing that the lattice is no longer connected. For systems diluted beyond the percolation threshold, it is meaningless to analyze measures of long range order (Grest and Gabl, 1979).

In 1982, Fernández, Andérico, and Streit began looking at the entropy density of this system (Fernández et al., 1982; Andérico et al., 1982). They used a transfer-matrix calculation to show that the minimum of the residual entropy occurs for a dilution of around 10% of the lattice, well below the percolation threshold.

A new avenue of study for this model was paved when Choy and Sherrington found the exact probability distribution of local fields $P(h)$, where h is the effective field acting on a site due to the interactions with its nearest neighbors, for the undiluted system (Choy and Sherrington, 1983a,b). A Monte Carlo calculation of $P(h)$ for the diluted case (Crewick et al., 1985) showed a local minimum in the distribution at $h = 0$ – this is called a "zero-field hole." Then, an exact transfer-matrix calculation (using a finite lattice) showed that the derivative of entropy density with respect to spin concentration x at $k_B T/J = 0$ and $x = 1$ (maximum concentration) is $k_B[\ln 2 - \ln P(0)]$ (Farach et al., 1988)

$$\left.\frac{\partial s}{\partial x}\right|_{x=1} = 1.9309\, k_B, \quad \text{for } \frac{k_B T}{J} = 0. \tag{2}$$

Note that this is the correct value as a numerical error appears in the result quoted in the Farach article (see Gonçalves et al. 1997). The rate by which the residual entropy drops as dilution is introduced is significantly greater than the linear approximation between the known $d = 0$ and $d = 1$ limits (see Figure 29 in Section 5.2). This steep slope is taken to indicate that the model has a strong tendency to order when diluted.

A triangular lattice decomposes into three *sublattices*, i.e. subsets of the lattice which are neighbored only by sites in the other sublattices (see Figure 1). Recently Kaya and Berker analyzed a model in which sites are randomly diluted on only one sublattice (Kaya and Berker, 2000). We shall refer to the lattice on which dilution occurs as sublattice A; the other two sublattices are B and C. For this model we measure dilution strength d as the fraction of sites removed from Sublattice A. Thus, a dilution of 1 corresponds to a lattice in which Sublattice A is removed entirely,

resulting in a honeycomb lattice. This model, which we shall refer to as the Kaya-Berker model, has the advantage that it remains connected even at full dilution, unlike the model of Grest and Gabl. As we shall see in Chapter 5 the Kaya-Berker model has the property that the residual entropy monotonically decreases with dilution.

Using hard-spin mean field theory (Netz and Berker, 1991a,b), Kaya and Berker looked at the critical behavior of this model (Kaya and Berker, 2000). They found that the model orders at finite temperature for a dilution strength at or above approximately $d \approx 4.2\%$. The nature of this order is as follows: sublattices B and C spontaneously magnetize with opposite signs and equal magnitudes, and spin-glass ordering occurs on sublattice A as indicated by a non-zero value of the Edwards-Anderson order parameter (see Section 4.2 for the definition of this quantity). Physically, the addition of vacancies to the two-dimensional case relieves frustration and leads to this ordered phase (Kaya and Berker, 2000). Thus, this model system provides an example of order arising from disorder and offers a generic system to explore the interplay between geometric frustration and randomness. This system exhibits spin-glass and magnetic ordering on separate sublattices, so its phase diagram possesses an unusual richness for a two-dimensional, short-range model.

CHAPTER 3

BACKGROUND

This chapter defines the statistical mechanical and information theoretic quantities that we have used to investigate phase transitions and ordering in the Ising antiferromagnet with quenched dilution on a triangular lattice. Included are discussions of traditional thermodynamic measures, such as the specific heat, magnetization, magnetic susceptibility, and entropy, as well as the excess entropy, an information theoretic measure of complexity that we have applied to this system. We have conducted this investigation within the canonical ensemble, thus assuming that the system is in thermal equilibrium and that the probability of a particular microstate is proportional to $e^{-\beta\mathcal{E}}$, where $\beta = \frac{1}{k_B T}$ and $\mathcal{E}$ is the energy of the microstate.

3.1 Specific heat and magnetic susceptibility

The specific heat is defined as the derivative of the internal energy density with respect to temperature T. The internal energy $\langle\mathcal{E}\rangle$ is the average over the thermal fluctuations of the microstate value, $\mathcal{E}$. Then:

$$c \equiv \frac{\partial\langle\mathcal{E}\rangle}{\partial T}. \tag{3}$$

For a system in thermal equilibrium (e.g., Reif 1965),

$$c = k_B\beta^2\left(\langle\mathcal{E}^2\rangle - \langle\mathcal{E}\rangle^2\right). \tag{4}$$

Thus the variance in the energy is proportional to $\frac{\partial\langle\mathcal{E}\rangle}{\partial T}$.

For the system under scrutiny here, the magnetization of the lattice is a natural variable to consider. The total magnetization is defined as the sum of all of the spins

in the lattice N,

$$M = \sum_{i=1}^{N} \sigma_i. \tag{5}$$

A straightforward calculation gives:

$$\langle M^2 \rangle - \langle M \rangle^2 = \frac{1}{\beta} \frac{\partial \langle M \rangle}{\partial H}. \tag{6}$$

Since the magnetization depends on the size of the system, it is an *extensive* property. It is often more convenient to work with the magnetization per site, or the *magnetization density* m, which is intensive. We denote an intensive quantity with the lower case letter corresponding to the capital letter that denotes its associated extensive quantity. To make Eq. 6 contain only intensive quantities, we divide both sides by the N^2, where N is the number of spins in the lattice. We call the response of $\langle m \rangle$ to changes in H the (intensive) magnetic susceptibility χ, and it is found by Eq. 6 to be

$$\chi = \frac{\partial \langle m \rangle}{\partial H} = \beta N (\langle m^2 \rangle - \langle m \rangle^2). \tag{7}$$

3.2 Thermodynamic entropy density

In studying heat engines, Rudolph Clausius found that the ratio of the amount of heat energy a heat engine gains from its environment to the temperature at which this heat gain occurred, has the properties of a state function (Clausius, 1865). A state function is a physical quantity that characterizes the state of a system, independent of its history. When an infinitesimal amount of heat $đq$ flows into a system, the infinitesimal change in its entropy dS is defined as this heat energy divided by the absolute temperature T at which the change occurred:

$$dS \equiv \frac{đq}{T}. \tag{8}$$

The cross through the infinitesimal indicates that q itself is not a state function and therefore it cannot be integrated directly, i.e. it is absurd to discuss the heat of the

system. For systems of constant volume or pressure, the infinitesimal heat gain $đq$ raises the temperature by dT and is related to the heat capacity C

$$đq = C\ dT. \tag{9}$$

Thus the entropy is often found via the temperature integral of the ratio of the specific heat c to the temperature itself

$$S(T) - S(T_0) = \int_{T_0}^{T} \frac{C(T')}{T'} dT' \tag{10}$$

where T_0 is a reference temperature. By dividing both sides by N, one obtains the intensive version of this equation, which yields the entropy density from an integral involving the specific heat. To use this approach $C(T)$ must be continuous and integrable.

Eq. 10 comes from the macroscopic interpretation of entropy and only describes how entropy changes and how this change can be determined. To describe the local origin of entropy, the concept of probability must be adopted. In the 1870's, a microscopic definition of entropy was provided by Max Planck and Ludwig Boltzmann, and independently by J. Willard Gibbs (Planck, 1959; Bolzmann, 1877; Gibbs, 1902). Their *statistical* definition of the entropy of a system which is at a given energy, one described by the microcanonical ensemble, is depicted in Figure 2[1] .

Figure 2: Boltzmann's tomb

Around 1900 Gibbs developed the notion of an ensemble which ultimately gave statistical mechanics a firm footing. An ensemble is a collection of identical systems, each in a different initial microstate selected according to the ensemble's probability distribution. With this framework of probability he came to the following formula for

[1]http://www-gap.dcs.st-and.ac.uk/ history/PictDisplay/Boltzmann.html

the entropy:

$$S = -k_B \sum_i p_i \ln(p_i), \tag{11}$$

where p_i is the probability of a microstate and the sum runs over all allowed microstates. It must be noted that Boltzmann and Thompson arrived at the same microscopic formula for the entropy density at about the same time. Boltzmann's formulation was so deeply rooted in the abstractness of probability theory, however, that it is the conceptual use of ensembles that has survived the test of time. The microscopic formulation of the entropy provides a link between the thermodynamical (macroscopic) state function and the physical building blocks that underlie it. Since a direct calculation using Eq. 11 requires sampling a huge number of microstates, it is too cumbersome to use in most situations.

3.3 The Shannon entropy

Claude E. Shannon introduced information theory in his monumental 1948 paper, "A Mathematical Theory of Communication" (Shannon, 1948). He considered streams of electrical pulses on a wire as information sources that transmitted pictures, words, and sounds. The streams he called *signals*, the pulses he called *bits*, and the wires he called *channels*. By regarding entropy as the amount of uncertainty or randomness in a signal, Shannon showed that by adding extra bits to a signal, transmission errors can be corrected. This conception of entropy paved the way for a new means of calculating the thermodynamic entropy of a large class of systems.

Shannon's analysis required the determination of the "amount of uncertainty in a probability distribution." This uncertainty is now known as the *Shannon entropy* H. To get a quantitative measure of the uncertainty of a probability distribution, Shannon required the following:

1. H must be maximized for a uniform distribution;

2. H must be a continuous function of the probability distribution. An infinitesimal change in the probabilities must cause an infinitesimal change in H; and

3. H must be independent of how the events are grouped.

These three requirements determine H *uniquely* to within a constant (Shannon, 1948; Khinchin, 1957; Cover and Thomas, 1991). For a finite set of N binary stochastic variables, $\sigma_i \in \{-1, +1\}$,

$$H(N) = -k_B \sum_{\sigma_1, \sigma_2, ..., \sigma_N} p(\sigma_1, \sigma_2, ..., \sigma_N) \ln p(\sigma_1, \sigma_2, ..., \sigma_N) \tag{12}$$

where $p(\sigma_1, \sigma_2, ..., \sigma_N)$ is the probability of the set of variables and the N summations account for all 2^N combinations of values of the variables exactly once. The Shannon entropy is a measure of the uncertainty of the N spins. For a uniform distribution, the Shannon entropy obtains its maximum. Conversely, if the spins are all up (or down), only one outcome is possible and the Shannon entropy vanishes.

For stationary processes in one dimension, the Shannon entropy H varies with the number of variables L as depicted in Figure 3 (Crutchfield and Feldman, 2003, and references therein). $H(0)$ is defined to be 0, as in this case there is no variable about which to be uncertain. A *stationary process* is a set of stochastic variables whose joint probability distribution is translationally invariant,

$$p(\sigma_1, \sigma_2, ..., \sigma_n) = p(\sigma_{1+k}, \sigma_{2+k}, ..., \sigma_{n+k}) \quad \text{for all } n \text{ and } k. \tag{13}$$

Since $H(L)$ asymptotically approaches linearity in L (Cover and Thomas, 1991; Crutchfield and Feldman, 2003), for a stationary process in one dimension $H(L)/L$ asymptotically approaches a constant. This constant, the slope of the dashed line in Figure 3, equals the thermodynamic entropy density s

$$s = \lim_{L \to \infty} \frac{H(L)}{L}. \tag{14}$$

Since $H(L)/L$ is slow to converge as L increases, we focus our attention on the L-dependent *entropy rate* $\Delta H(L)$. As the number of variables is discrete, the slope of

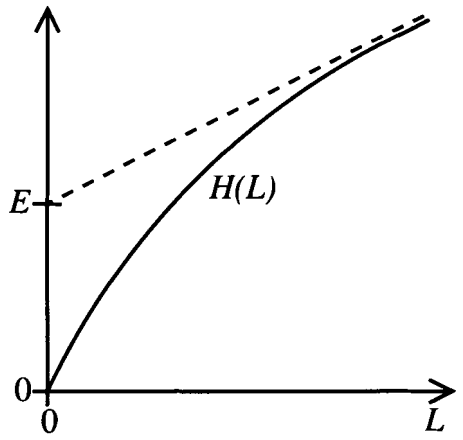

Figure 3: Shannon entropy $H(L)$ vs. number of stochastic variables L for a stationary process in one dimension (Crutchfield and Feldman, 2003). In the large variable limit, the slope of the dashed line in the figure represents the physical entropy density s.

$H(L)$ at any L in Figure 3 is calculated by considering two consecutive points $(L-1)$ and L. Using set notation the Shannon entropy (Eq. 12) is denoted $H\big[\{\sigma_i : 1 \leq i \leq L\}\big]$, thus,

$$\Delta H(L) = H\big[\{\sigma_i : 1 \leq i \leq L\}\big] - H\big[\{\sigma_i : 2 \leq i \leq L\}\big]. \tag{15}$$

The probability distribution in the second term of Eq. 15 differs from the first in that spin σ_1 is removed. Thus, while the sum in the first term is over 2^L configurations, the sum of the second term is over 2^{L-1}. For a stationary process in one dimension $\Delta H(L)$ converges to the thermodynamic entropy in the large variable limit (Cover and Thomas, 1991; Crutchfield and Feldman, 2003)

$$s = \lim_{L\to\infty} \Delta H(L). \tag{16}$$

In addition to the L-dependent Shannon entropy rate, the *conditional Shannon entropy* also provides an alternate method to obtain the thermodynamic entropy. In order to calculate the conditional Shannon entropy we need to single out one of the spins as a *target spin* and a neighboring block of spins is called the *conditional set.* For a set of L spins, each of which is denoted by σ_i, the conditional Shannon entropy

of the target spin, say σ_1, is

$$H[\sigma_1|\{\sigma_i : 2 \leq i \leq L\}] = -k_B \sum_{\sigma_1,\sigma_2,...,\sigma_N} p(\sigma_1, \sigma_2, ..., \sigma_N) \ln p(\sigma_1|\sigma_2, ..., \sigma_N) \qquad (17)$$

where $p(\sigma_1|\sigma_2, ..., \sigma_N)$ is the probability spin σ_1 takes a value of 1 or -1 (depending on which term of the sum) given the values of the variables in the conditional set. The conditional Shannon entropy can be interpreted as the average uncertainty of the orientation of the target spin given the state of the spins in the conditional set.

Using the fact that the conditional probability $p(x|y)$ equals $\frac{p(x,y)}{p(y)}$, it is straightforward to show that $\Delta H(L) = H[\sigma_1|\{\sigma_i : 2 \leq i \leq L\}]$. Eq. 16 may thus be rewritten as:

$$s = \lim_{L\to\infty} H[\sigma_1|\{\sigma_i : 2 \leq i \leq L\}]. \qquad (18)$$

The set of L stochastic variables referred to in Eqs. 12, 17, and 18 is a subset of the spins called a *shape*. Together, the target spin and the conditional set constitute the shape. The conditional Shannon entropy tells us the average uncertainty of the orientation of the target spin, given the knowledge of the orientation of the other spins in the shape.

In two dimensions a similar result holds, but one must use considerable care when defining the set of variables upon which the target spin is conditioned, see Feldman and Crutchfield 2003, and references therein. The limit in Eq. 18 converges differently for different choices of shape; some choices will not converge at all and the limit does not hold. To determine the set of spins that converges to the entropy density and does so efficiently, we require that the target spin be "shielded" from one half of the lattice (Goldstein et al., 1990). A target spin is *shielded* from another by a set of spins if the target spin's probability distribution depends only of the values of the spins in the set, and not additionally on the value of the other. For infinite range interactions, those for which any spin affects any other, the set of spins must then be the whole lattice, making the direct computation of the entropy using Eq. 18 impractical. However,

for models in which the interactions between spins are of finite range, we only need to use a set of variables that are connected along one dimension and extend as far as the interaction range in the other direction (Alexandrowicz, 1971, 1976; Schlijper and Smit, 1989; Schlijper et al., 1990; Eriksson and Lindgren, 1989). For models with only nearest-neighbor interactions, as is the case for the models studied here, we can thus use a shape that is one spin thick and connected and extends along one dimension. The appropriate set of spins for the two-dimensional Ising model on a triangular lattice, including the target spin, is shown in Figure 4. The figure shows the shape for $L = 7$. As the shape grows, spins are added to the left and right ends of the shape.

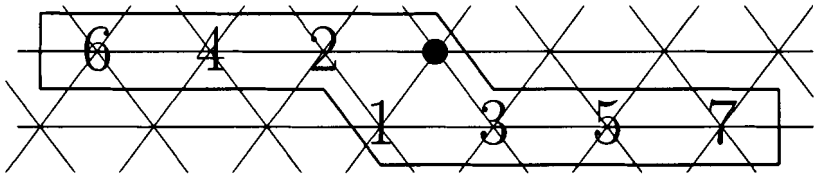

Figure 4: A shape of eight sites for the Ising model on a triangular lattice used in the calculation of the Shannon entropy. The target spin is marked with the '•' .

The "kink" in the shape of Figure 4 around the target spin achieves shielding by including at least half of its nearest neighbors. In the limit in which the shape extends infinitely far to the left and right, the target spin is shielded from all those beneath it. This approach, whose accuracy is well established for systems without frustration (Alexandrowicz, 1971, 1976; Meirovitch, 1977, 1983a; Schlijper, 1983; Schlijper et al., 1990; Schlijper and Smit, 1989; Goldstein et al., 1990; Meirovitch, 1999), allows one to express the entropy of the lattice as a function of the frequencies of occurrence of configurations in a small neighborhood of spins. These frequencies can be directly measured in a Monte Carlo simulation, allowing us to collect the probability distribution required by Eq. 12 for any temperature. The probability distribution is formed by building a histogram of the occurrences of configurations.

The infinite shape-size limit in Eq. 16 cannot, of course, be done in practice. However, it turns out that $\Delta H(L)$ converges extremely quickly to its large-L value (see, e.g., (Meirovitch, 1999)). The well known information theoretic method of using the conditional Shannon entropy for calculating the thermodynamic entropy density s has been applied successfully to a number of different systems, including: the two-dimensional Ising model and the $q = 5$ two-dimensional Potts model (Schlijper and Smit, 1989); the Ising model on a simple cubic lattice (Meirovitch, 1983a); a two-dimensional hard-square lattice gas (Meirovitch, 1983b); the three-dimensional fcc Ising antiferromagnet (Meirovitch, 1984); coupled map lattices (Olbrich et al., 2000); Gaussian random fields (Marčelja, 1996); polymer chain models (Meirovitch, 1999); and network-forming materials (Vink and Barkema, 2002).

To estimate the entropy we calculate $\Delta H(L)$ for a suitably large L. This is done by calculating $H\big[\{\sigma_i : 1 \leq i \leq L\}\big]$ (which uses the probability distribution formed by joining all the spins in the shape) and subtracting from it $H\big[\{\sigma_i : 2 \leq i \leq L\}\big]$ which is found using the probability distribution formed by joining all the spins in the conditional set. Thus $\Delta H(7)$ is found by first collecting a normalized histogram of configurations for the shape of Figure 4. We then calculate $H(7)$ via Eq. 12, forming subsequently a new normalized histogram by reducing the original to one where the target spin is removed. We calculate $H(7-1)$, and then subtract it from $H(7)$ to get $\Delta H(7)$. In Figure 5 we see that the value of $\Delta H(L)$ is very close to its large L value by the length $L = 5$. All the information theoretic measurements of entropy in this thesis were collected via $\Delta H(10)$.

3.4 Excess entropy

In the early and mid eighties the *excess entropy*, also called "stored information," "effective measure complexity," and simply "complexity," was put forth as a measure of a system's regularities and structure (Crutchfield and Packard, 1983; Shaw, 1984;

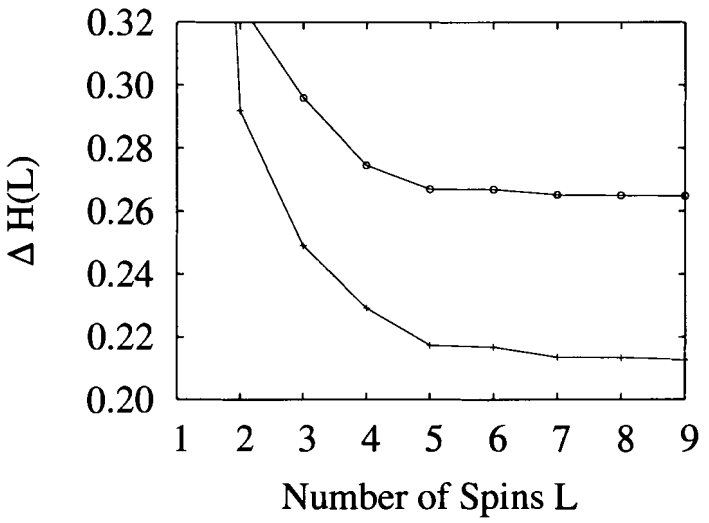

Figure 5: Two samples of the L-dependent entropy rate $\Delta H(L)$ vs. the number of spins in the shape L for a system where sublattice A is 10% diluted. The value of $\Delta H(L)$ is very close to its large L value by the length $L = 5$. The top curve is for $k_B T/J = 0.6$. The bottom curve is for $k_B T/J = 0.8$

Grassberger, 1986; Szépfalusy and Györgyi, 1986). The excess entropy has been applied successfully in a number of settings (Lindgren and Norhdal, 1988; Nemenman, 2000; Bialek et al., 2001; Feldman, 1998; Feldman and Crutchfield, 1998; Crutchfield and Feldman, 2003; Feldman and Crutchfield, 2003). Although E is not a metric invariant, it has been established as a general measure of the complexity or structure of physical systems (Crutchfield and Feldman, 2003, and references therein).

The excess entropy is a measure of how the slope of $H(L)$ in Figure 3, $\Delta H(L)$, converges to its limit, the thermodynamic entropy. The slope $\Delta H(L)$, for finite L, overestimates s because single measurements appear more random for finite L than they really are. Thus the amount of randomness (i.e. information) reported for a shape of finite length by Eq. 15 that is actually due to correlations is the area between the $\Delta H(L)$ and s curves in Figure 6. This discrete integral has the following form:

$$E = \sum_{L=1}^{\infty} (\Delta H(L) - s) . \tag{19}$$

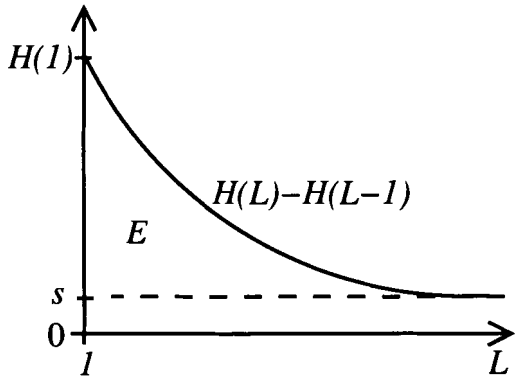

Figure 6: Schematic plot of L-dependent entropy rate $\Delta H(L)$ vs. number of stochastic variables L for a stationary process (Crutchfield and Feldman, 2003). In the large variable limit $\Delta H(L)$ is the thermodynamic entropy density s.

The excess entropy is also equal to the $L = 0$ intercept of the dotted line in Figure 3. Thus,

$$\begin{aligned} E &= \sum_{L=1}^{\infty} (\Delta H(L) - s) \\ &= \big(H(1) - H(0) - s\big) + \big(H(2) - H(1) - s\big) + ... \\ &= \lim_{L \to \infty} \big(H(L) - sL\big). \end{aligned} \tag{20}$$

That is,

$$H(L) = sL + E \quad \text{in the limit } L \to \infty. \tag{21}$$

CHAPTER 4

METHODS

This chapter describes the Monte Carlo simulation performed to investigate phase transitions and ordering in the Ising antiferromagnet with quenched dilution on a triangular lattice. Exact results are virtually unattainable for this system due to its geometric inhomogeneity and rugged frustration. Thus we choose to probe it with a Monte Carlo simulation. Below we give the details of the Metropolis algorithm, a Markov process satisfying the conditions of detailed balance and ergodicity that generates a dynamic pathway through state space such that states are visited with a frequency proportional to their Boltzmann weight (Newman and Barkema, 1999). Then we discuss the equilibration time of the system, the correlation time of the system, critical slowing down of the system, and the calculation of thermodynamic variables. The information theoretic method of calculating the entropy is described in addition to the conventional one. The errors of these measurements are also analyzed.

4.1 Importance sampling

To obtain reliable average values of thermodynamic variables, we need to sample the states of the system according to their Boltzmann weights. This is can be achieved via the technique of *importance sampling* according to which the states generated by our Monte Carlo algorithm occur with a probability proportional to that specified by the canonical ensemble. The *Metropolis algorithm* (Metropolis et al., 1953) achieves this by flipping the spins one at a time, a process known as *single-spin-flip dynamics.* Single-spin-flip dynamics tends to keep the system in states of approximately the same energy for long periods of time.

The algorithm is to select a spin at random, flip it with a probability $P_{\nu\mu}$ given by Eq. 22, and repeat.

$$P_{\nu\mu} = \begin{cases} e^{-\beta(\mathcal{E}_\nu - \mathcal{E}_\mu)} & : \quad (\mathcal{E}_\nu - \mathcal{E}_\mu) > 0 \\ 1 & : \quad \text{otherwise} \end{cases} \tag{22}$$

where $\mathcal{E}_\mu$ is the energy of the current state μ and $\mathcal{E}_\nu$ is the energy of the state ν that the system would be in if the chosen spin is flipped. The Metropolis algorithm dictates that, if the flipping of a site causes the lattice to be in a state of higher energy, the flip is accepted according to the Boltzmann probability whereas the flip is always accepted if the lattice energy is decreased by the flip.

The spins are flipped according to *transition probabilities* $p_{\mu\nu}$, the probability of going from state μ to state ν. These probabilities must be chosen so that the condition of *ergodicity* is satisfied. Ergodicity, required to ensure that time averages are equal to ensemble averages, is satisfied when there is a finite path from any state μ to any other state ν. Since the transition probability between any pair of states in Eq. 22 never vanishes, the condition of ergodicity is satisfied. The condition of *detailed balance*, which ensures that the system obeys time-reversal symmetry when in equilibrium, is satisfied when the transition probabilities $p_{\mu\nu}$ have the following property:

$$\frac{p_{\mu\nu}}{p_{\nu\mu}} = e^{-\beta(\mathcal{E}_\nu - \mathcal{E}_\mu)} \tag{23}$$

where $\mathcal{E}_\mu$ and $\mathcal{E}_\nu$ are the energies of states μ and ν respectively and β is the inverse temperature (scaled by Boltzmann's constant). By comparing Eq. 22 and Eq. 23, we see that the Metropolis algorithm trivially satisfies the condition of detailed balance.

In short, the process defined by the Metropolis algorithm moves the lattice through microscopic configurations consistent with the specified temperature, yielding a state probability distribution converging to that specified by the canonical ensemble. Namely, the probability of a configuration c is proportional to $e^{-\beta\mathcal{H}(c)}$, where $\mathcal{H}(c)$ is the energy of the configuration c.

4.2 Details of the system we used

Monte Carlo simulations require many measurements to be taken at each temperature. After completing these measurements, we perform the analysis, store the results, increment the temperature, and repeat. It must be noted that exactly the same results are found by holding the temperature constant and incrementing the interaction strength J. In that implementation the system orders for large J, and below the critical strength J_c the system is disordered.

4.2.1 Lattice specification

Since the model is on a triangular lattice, each site has six nearest neighbors (see Figure 1). We store the lattice as a one-dimensional array and use helical boundary conditions (for details see Newman and Barkema, 1999). The order of the sites in the array corresponds to the three sublattices stored one after the other. Thus, every third entry is in the same sublattice. For each spin to have nearest neighbors of unlike sublattice, we restrict the lattice to $(L-1)$ columns, where L is a multiple of three. Further, to achieve sublattice matching at the boundaries, the number of rows must also be a multiple of three. Thus the array must be of length $L(L-1)$. The lattice used for all of the data reported in this thesis is of size 98×99.

4.2.2 Equilibration time

Starting at a new temperature requires waiting for the system to reach equilibrium. To get a sense of the time required for the system to come to equilibrium, we look at plots of the magnetization density as a function of time starting from an initial lattice that corresponds to an infinite temperature, disordered lattice (see Figure 7). The way we characterize time is in units of Monte Carlo steps, or MCS. If the lattice of the simulation has 10^4 sites, one MCS corresponds to 10^4 randomly proposed spin flips of the Metropolis algorithm. Guided by outputs like those in Figure 7, we

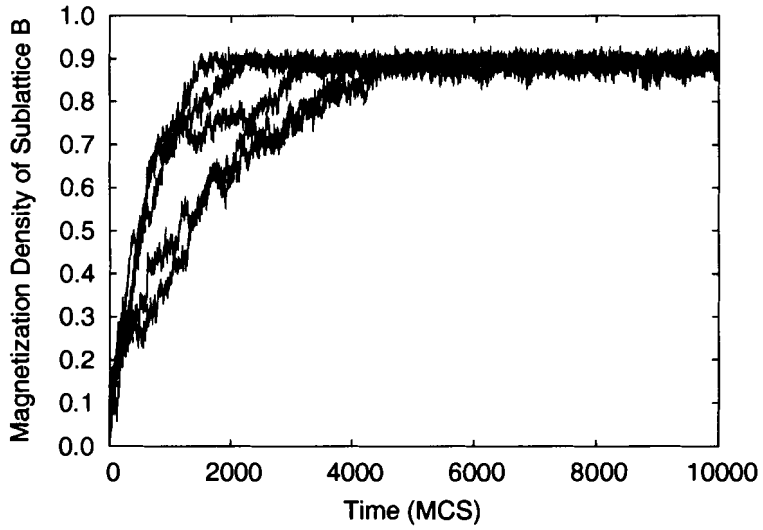

Figure 7: Magnetization density of sublattice B m_B vs. time t from five simulations for a lattice that has sublattice A 50% diluted at $k_BT/J = 1.0$. To ensure a conservative estimate of the equilibration time, these simulations were started with a random lattice (corresponding to $T \rightarrow \infty$) and equilibrated to a temperature just below the critical temperature $k_BT/J = 1.2$. Note that after a transient time of around $4,000\,MCS$, the system equilibrates and the magnetization curve levels off. Once equilibrated, the fluctuations in the magnetization are due to the thermal fluctuations and are independent of the initial condition.

discarded the first $4000\,MCS$ after each increment of T for all for all runs reported in this thesis to ensure equilibrium.

4.2.3 Correlation time

Once the system is in equilibrium, the time between measurements should be large enough so that successive measurements are sufficiently uncorrelated to contribute new information. To estimate the correlation time τ, the number of Monte Carlo steps required to go from one state to another that has the orientation of all spins significantly independent of the previous state, we form the time-displaced autocorrelation function for a single spin at a single site, a variant of the Edwards-Anderson

order parameter (Edwards and Anderson, 1975)

$$q(t) = \frac{1}{N}\sum_{i=1}^{N}\langle(\sigma_i(0) - m_i) \times (\sigma_i(t) - m_i)\rangle, \tag{24}$$

where m_i is the average magnetization of spin σ_i. For the system under scrutiny here, we look at this Edwards-Anderson order parameter variant for each sublattice independently. For sublattice A, m_i is zero for all sites so $q_A(0) = 1$. In Figure 8 we see this function decays exponentially above approximately 20 MCS, i.e. $q(t) = e^{-}t/\tau$ above 20 MCS. The correlation time τ is equal to the area under the $q(t)$ curve:

$$\tau = \int_0^\infty q(t')dt'. \tag{25}$$

Figure 9 shows two different results of integrating $q(t)$.

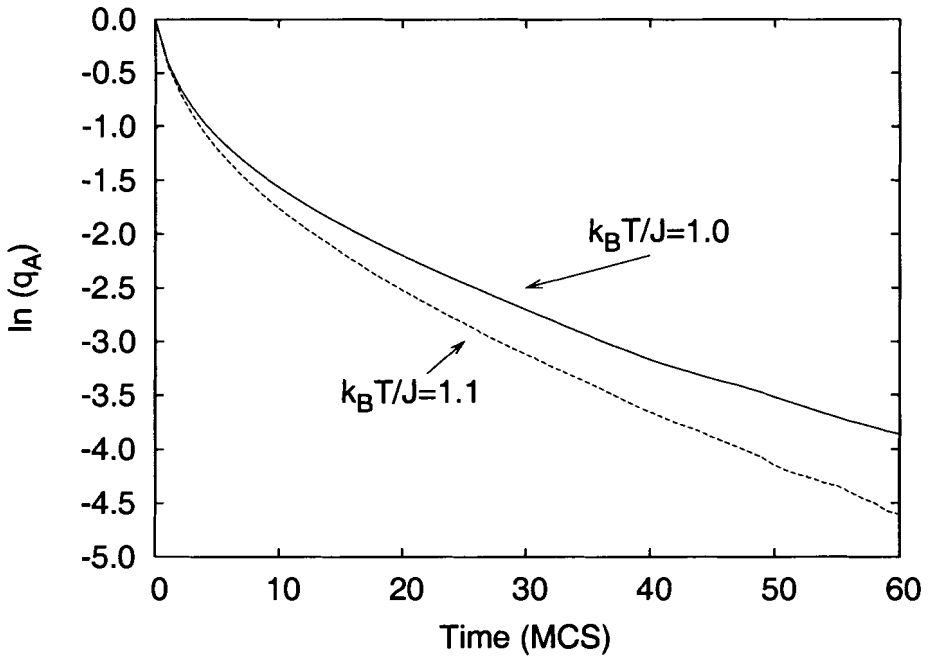

Figure 8: The log of the Edwards-Anderson order parameter of sublattice A, $ln\,(q_A)$, vs. time t on the undiluted lattice. For $k_BT/J = 1.1$ the data is plotted with a dashed curve while for $k_BT/J = 1.0$ a solid curve is used.

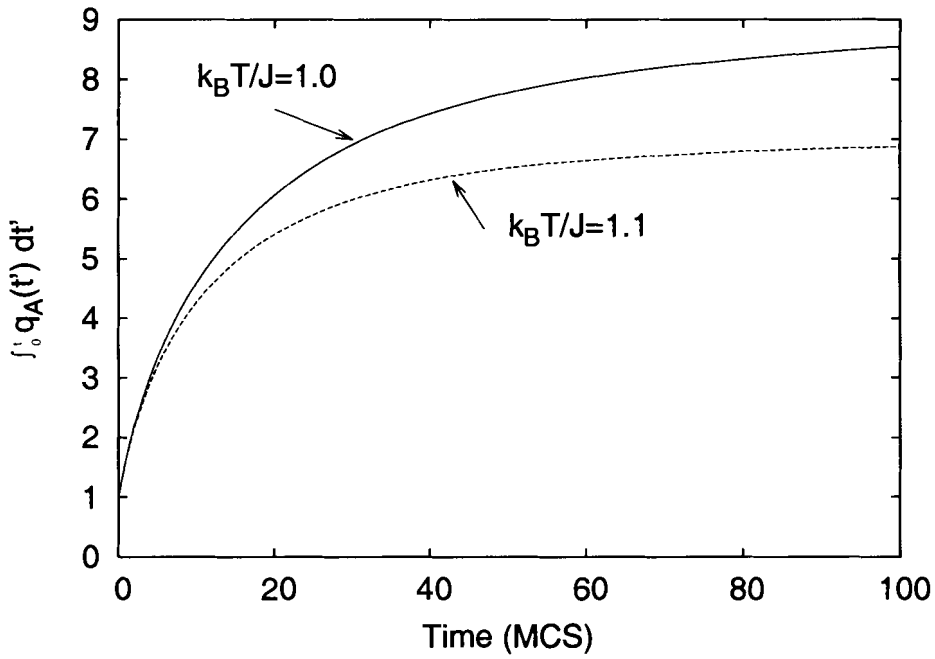

Figure 9: Integral of the Edwards-Anderson order parameter of sublattice A, $\int_0^t q(t')dt'$, vs. time t This data was taken on undiluted lattice for $k_BT/J = 1.1$ (dashed curve) and $k_BT/J = 1.0$ (solid curve).

The Metropolis algorithm for the Ising model is an excellent algorithm well away from the critical temperature, but in the limit as temperature approaches T_c and the system size goes to infinity, the number of Monte Carlo steps required to obtain an uncorrelated lattice diverges (Newman and Barkema, 1999). Andérico, Fernández, and Streit explored the slowing down in the systems of Grest and Gabl (1979) by integrating q(t) to estimate τ (1982). They showed the extent to which the Metropolis algorithm on this system slows down as the temperature drops by fitting the function

$$\tau = e^{A(T-T_c)^{-C}} \tag{26}$$

to their data for various values of critical temperature T_c. Using a lattice of roughly twice the side length of theirs (50×50), we verified the results of Andérico et al. (see Figure 10). For $T_c = 0$ they report $A = 2.37$, $C = 1.01$ (Andérico et al., 1982, Figure 7), and we find $A = 2.31 \pm 0.07$, $C = 1.12 \pm 0.07$, in excellent agreement with their results.

For the data collected for this thesis, sequential updating with measurements taken every $20\,MCS$ was used throughout. We average over many independent runs, thus providing error-bar estimates in the standard fashion.

4.2.4 Finite size and low temperature subtleties

Below the critical temperature, single-spin-flip dynamics provides a path for the lattice to flip over for a finite size lattice (Newman and Barkema, 1999). This global flipping could not occur in an infinite lattice. To get reliable estimates of the magnetization of the two undiluted sublattices in this region we must take the absolute value of the sublattice magnetizations. Above the critical temperature the absolute value is not required, and indeed skews the data. However, since the actual critical temperature is rarely known, we take the absolute value of the sublattice magnetizations for all temperatures. This causes the high temperature sublattice magnetization density values never to vanish (see Figure 11). Thus the analysis of magnetization

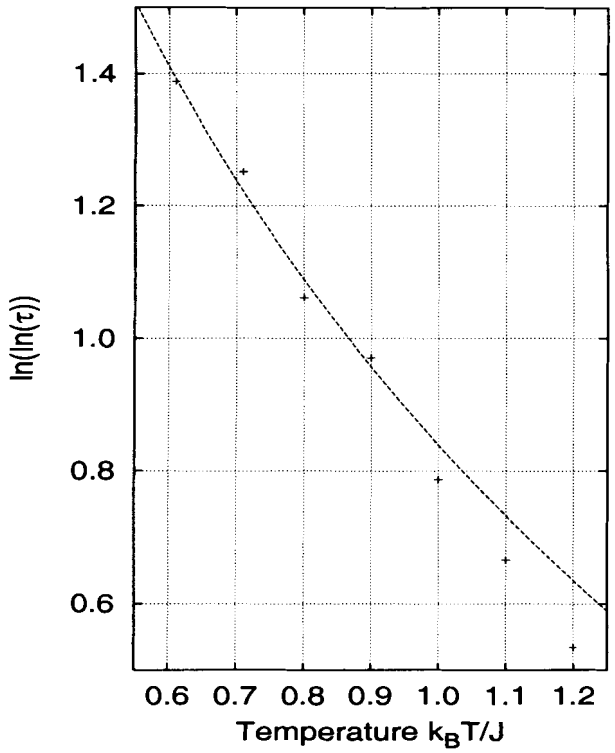

k_BT/J	$\tau(MCS)$
1.2	5.5
1.1	7
1.0	9
0.9	14
0.8	18
0.7	33
0.6	55

Figure 10: Correlation time τ vs. temperature k_BT/J for the undiluted case on a 98×99 lattice. The curve is a fit of Eq. 26 using $T_c = 0$.

densities alone is not necessarily the most reliable means to identify the location of critical temperatures.

An important limitation of this model is its behavior at low temperatures. For low dilutions this model is frustrated and thus has a rugged free energy landscape. As the system is cooled, Monte Carlo methods become inadequate at sampling the whole phase space. The algorithm becomes trapped in the vicinity of a local free energy minimum, leading to incorrect sampling probabilities and inaccurate data. In Section 5.1 we will make some practical inferences to identify the temperature where this method becomes unreliable, and we make a conservative estimate of this temperature to be sure to record only accurate results at temperatures for which the algorithm samples phase space representatively.

4.3 Entropy measurement

4.3.1 Traditional method

The standard method for calculating the entropy density of Equation 10 with a computer is via

$$s(T) - s(T_0) = \sum_{T'=T_0}^{T} \frac{c(T')}{T'} \delta T', \tag{27}$$

where δT is the temperature interval between our specific heat data points. To reduce errors arising due to approximating the integral as a sum, we need $\delta T'$ to be small. This is computationally expensive, however, so we need to optimize $\delta T'$ for tolerable error. As we shall see in Figure 13, the error is not immediately obvious. Thus we choose the moderate value $\delta T' = 0.02$ for the data collected via this method

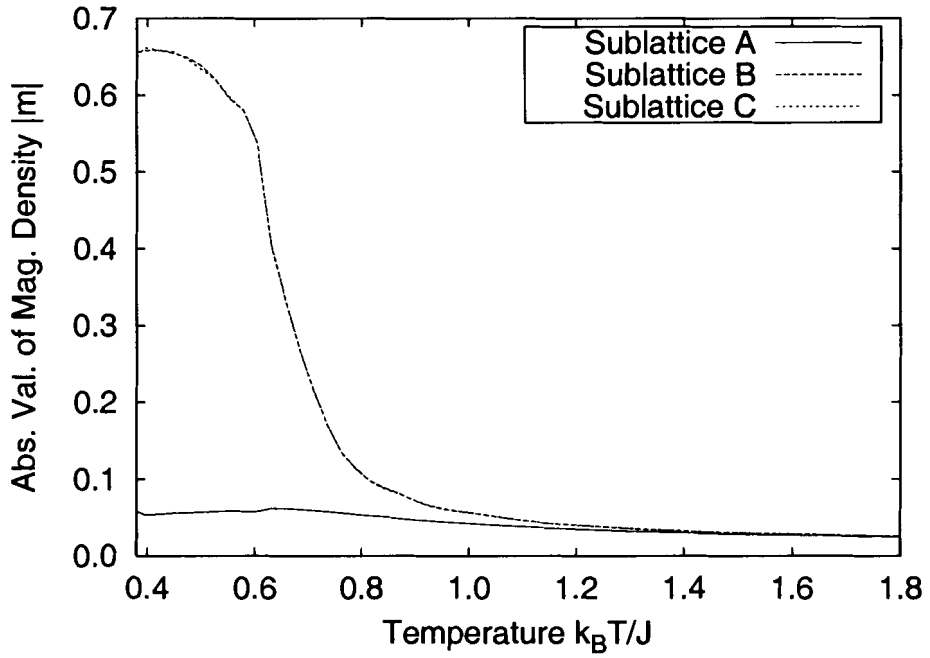

Figure 11: Absolute value of magnetization densities $|m_A|$, $|m_B|$, and $|m_C|$ vs. temperature k_BT/J. The data was taken on a lattice of 98 × 99 spins with 5% of Sublattice A randomly diluted. The values were found by averaging over 30,000 measurements. The magnetization appears to be non-zero above the critical temperature $k_BT/J \approx 0.63$. The curves for $|m_B|$ and $|m_C|$ lie almost directly on top of each other as expected.

in this research and focus on the error when we get to the information theoretic method. For the Kaya-Berker model the zero temperature entropy endpoint $s(T_0) = s(T = 0)$ is known for two limiting cases. For the honeycomb lattice ($d = 1$) the residual entropy density vanishes (all frustration is relieved and there is a vanishing multiplicity in the ground state), and for the triangular lattice ($d = 0$) it takes the value 0.323066 k_B (Wannier, 1950). We are interested in the entropy density for arbitrary dilution, for which the zero point entropy density is unknown. However, the infinite temperature limit provides an endpoint entropy we can calculate analytically. Thus only useful values of the entropy density provided by this method must start from the high temperature limit. For $T \to \infty$ the value of the entropy density can be determined via the Boltzmann relation; $S = k_B \ln W$ where W is the number of accessible states. For a system of N spins:

$$\begin{aligned} S(T \to \infty) &= k_B \ln(2^N), \\ s(T \to \infty) &= k_B \ln(2). \end{aligned} \tag{28}$$

Although the entropy in the infinite temperature limit is exact, in practice the simulation cannot start from infinity. We have used a high temperature expansion of the entropy to solve this problem. We let the ratio of low energy bonds N_- to high energy bonds N_+ be $e^{\beta 2J}$, since $2J$ is the energy change if one of the spins flipped and the bond became a low energy one. To first order in β, this exponential can be approximated as $1 - 2\beta J$:

$$\frac{N_-}{N_+} = 1 + 2\beta J. \tag{29}$$

For dilution d, the total number of bonds is related to the number of lattice sites as follows:

$$\begin{aligned} N_+ + N_- &= 3N - 6d\frac{N}{3} \\ &= (3 - 2d)N. \end{aligned} \tag{30}$$

Substituting Eq. 29 into Eq. 30, we find the number of high energy bonds.

$$\begin{aligned} N_+ + (1+2\beta J)N_+ &= (3-2d)N \\ N_+ &\approx \frac{(3-2d)N}{2}(1-\beta J) \end{aligned} \tag{31}$$

Now substituting Eq. 31 into Eq. 30 enables us to obtain the number of low energy bonds.

$$N_- \approx \frac{(3-2d)N}{2}(1+\beta J) \tag{32}$$

Thus the total internal energy, $(N_+ - N_-)J$, is:

$$U \approx -(3-2d)N\beta J^2. \tag{33}$$

We then use this formula to determine the specific heat to lowest order β:

$$\begin{aligned} c &= \frac{1}{N}\frac{\partial U}{\partial T} \\ &= -\frac{1}{Nk_BT^2}\frac{\partial U}{\partial \beta} \\ &\approx \frac{1}{k_BT^2}(3-2d)J^2 \\ \frac{c}{k_B} &\approx (3-2d)\left(\frac{J}{k_BT}\right)^2. \end{aligned} \tag{34}$$

This function is plotted with data in Figure 12.

Returning now to Eq. 27, note that the value of the entropy that this method provides at any given temperature is dependent on the preceding value. Thus the uncertainty of the value gets bigger as the simulation moves away from the high temperature limit. We take the value of c given by Eq. 34 at $k_BT/J = 30$, a reasonable choice balancing accuracy and computational efficiency, and use this as our starting point in the sum in Eq. 27. Figure 13 shows the results of ten simulations with different random seeds. The average of the specific heat was then calculated as well as its standard deviation σ_c at each temperature. The specific heat c fluctuates more and more as the critical temperature $k_BT/J \approx 0.76$ is approached, causing σ_c

to grow. The solid entropy curves in Figure 13 represent the integrals of $\frac{c \pm \sigma_c}{T}$ and can be interpreted as the maximum error of the entropy density. From this we see that, although the specific heat curve given by the high temperature expansion never lines up with the data in Figure 12, the curves are so close at $k_B T/J = 30$ that the high temperature error becomes negligible compared to that caused by numerical integration under the fluctuating specific heat curve.

In some systems the specific heat diverges and the integral cannot be performed reliably over the critical temperature. In these cases two integrals must be done, one from each end of the temperature range. The low temperature endpoint is usually not known and thus this method is not applicable in these regions.

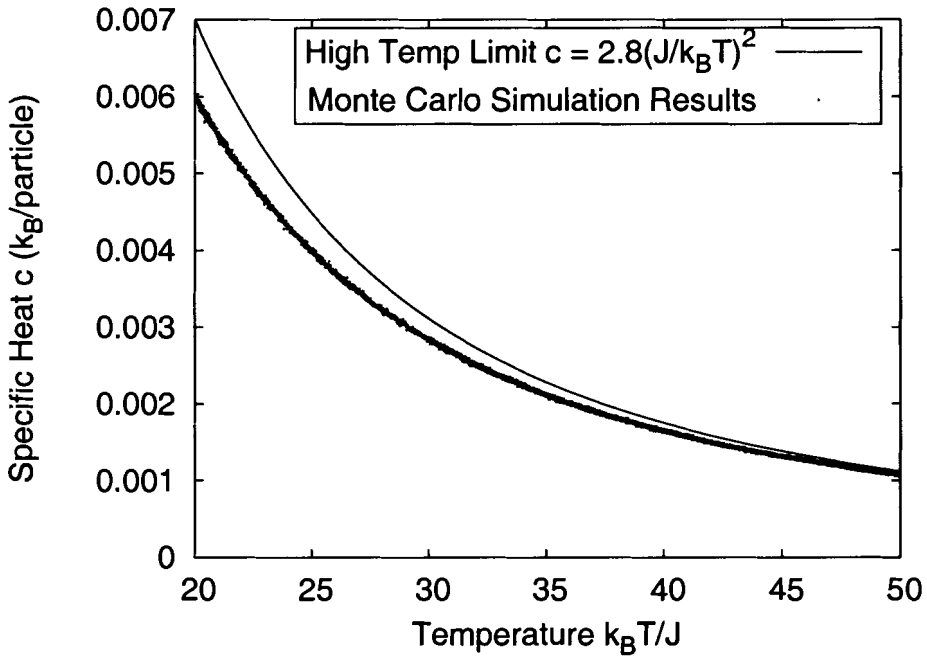

Figure 12: Specific heat c vs. temperature $k_B T/J$ at high temperature for the 10% diluted case. Note the small scale on the vertical axis.

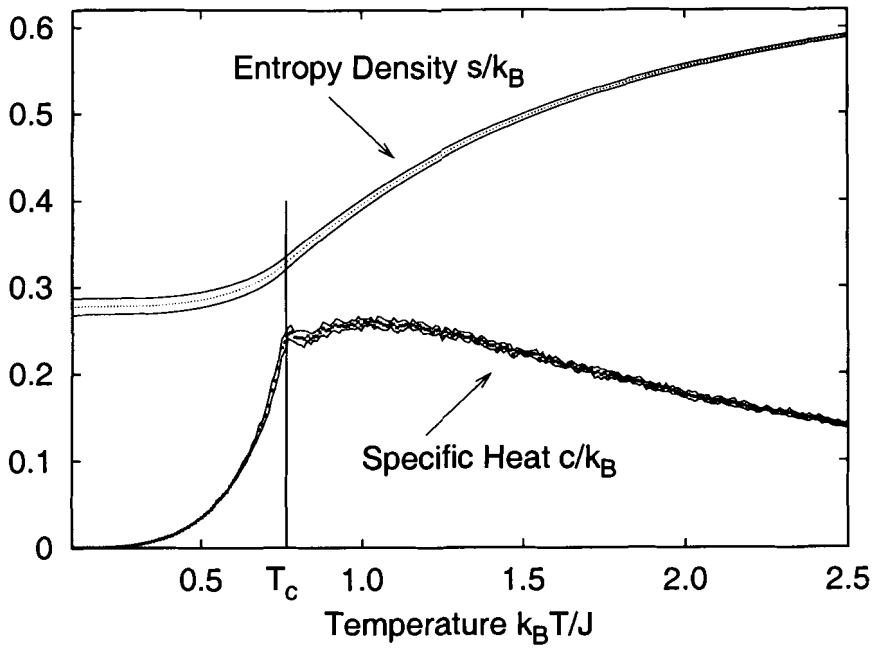

Figure 13: Specific heat averages and standard deviations for sublattice A diluted 10%. The error of the entropy is estimated by doing integrals of $c \pm \sigma_c$, as discussed in text.

4.3.2 Information theoretic method

We recall that the physical entropy density is found information theoretically by collecting histograms of the occurrences of configurations to use as probability distributions in Eqs. 12 and 16. As is often the case with disordered systems, in order to apply this method to the Kaya-Berker model, a crucial issue is at what stage in the calculation one performs an average. To adapt this information theoretic approach for disordered systems requires making a key modification. In the undiluted system, one sweeps the shape of Figure 4 through the lattice, noting occurrences of each shape configuration. We call this the *sweeping method* of collecting the histogram. The result is the frequency of occurrence of each configuration, averaged over the ensemble (via the Monte Carlo simulation) and averaged spatially over the lattice. However, in a disordered system, if one performs this latter average, one is also averaging over different local regions of diluted sites. In so doing, the randomness of the dilution gets

mixed with the fluctuations of the spin degrees of freedom, yielding a significantly overstated entropy for the system.

For this reason, instead of using the sweeping method, we keep the shape fixed at a number of selected sites, collecting separate histogram data at each site during the simulation. We call this the *planted method.* It preserves the effects of different local bond realizations. The result is a *local* entropy that measures the unpredictability of a particular single spin at a particular site, averaged over the statistical mechanical ensemble. The thermodynamic entropy density then is just the average of these "local contributions." In this research we estimate the entropy using this method by taking an average over 900 individual local entropy contributions. The decision to use 900 shapes was made in order to have enough shapes to sample a variety of realizations of the dilution without requiring excessive memory for histogram storage. It is important to realize that a local entropy is not a property of a single site but rather, it takes into account the degree to which a single site is (or is not) correlated with its cluster of neighbors. Specifically, it is the uncertainty of the orientation of the spin at that site, given the knowledge of the orientations of the spins in the cluster of Figure 4.

An important characteristic of the Kaya-Berker model is seen by looking at different realizations of the dilution. In Figure 14 the entropy densities from eleven independent simulations are shown as a function of time. Different spins in sublattice A get diluted in each disorder realization, yielding different entropy densities. We use a 98×99 lattice with a relaxation time of $20\,MCS$ (see Section 4.2) for the data of Fig. 14. Notice that the entropy density only rises from $0.44620k_B$ to $0.44665k_B$ (an increase of $\Delta s = 0.00045k_B$) between 500,000 counts and 5 million counts. It is thus clear that 500,000 counts are plenty to get precise measurements of the entropy den-

point and above $k_BT/J = 0.4$ and for all dilutions. The standard deviation of this

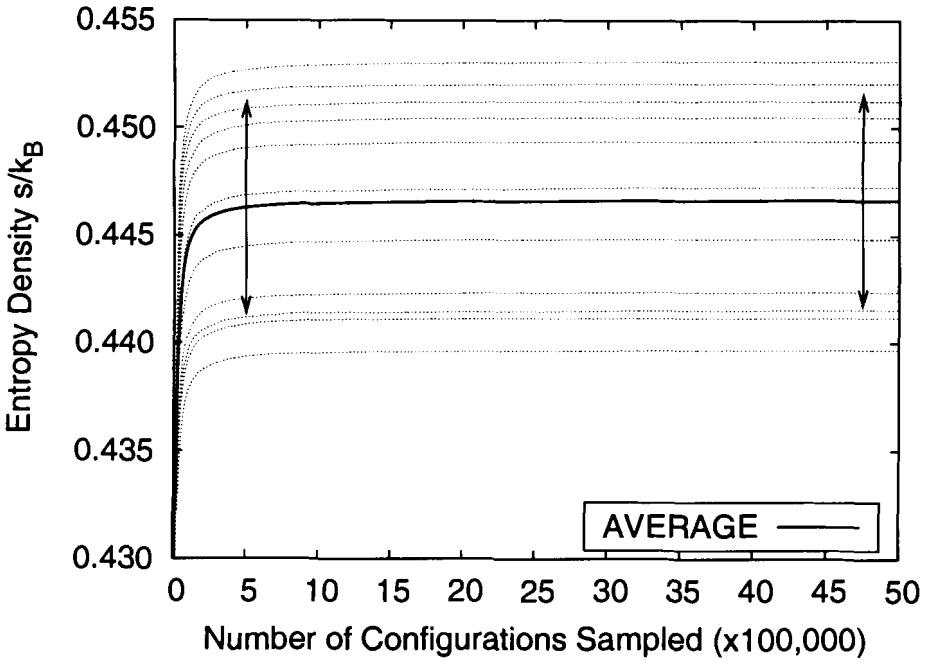

Figure 14: Entropy density vs. number of configurations sampled for different realizations of sublattice A diluted 10%. This data is for a temperature of $k_BT/J = 1.3$ – significantly above the critical temperature for this system. Note the narrow scale on the vertical axis.

variation is about $0.005k_B$ or about 1 % of the average entropy density for all temperatures. As is the case for all of the information theoretic results in this thesis, the entropy is calculated for each run by setting up 900 shapes placed in such a way that their target spins make a 30 × 30 rhombus. The entropy density depends on which sites are chosen for dilution. We ran several simulations of the same lattice with the same locations for the planted shapes, resulting always in very similar estimations of the average entropy density (less than 0.05 % error). On the other hand, eleven simulations were done on the same lattice but choosing different places to place the shape, resulting in the plot above.

CHAPTER 5

RESULTS

This chapter presents the results concerning the phase transitions and ordering in the Ising antiferromagnet with quenched dilution on a triangular lattice. Included are discussions the critical temperature, the magnetization critical exponent β, the Edwards-Anderson order parameter, and histograms. Then we discuss the traditional entropy calculations followed by the Shannon entropy calculations. We compare these two methods, and also show results for the excess entropy.

5.1 The phase transition

In this section we use the magnetization density and Edwards-Anderson order parameter to quantify the ordering in this model as a function of dilution. We also show how the probability distributions of the configurations of the spins in the shape used to calculate the Shannon entropy indicate the phase transition. We have not reported results for k_BT/J less than 0.4, since we found evidence of the system freezing into metastable states at lower temperatures, a common problem in simulations of models in which frustration is present (Grest and Gabl, 1979).

Figure 15 shows the behavior of the magnetization density as a function of temperature on each of the three sublattices and the whole lattice for the undiluted case. As expected, and in agreement with previous work (Domb and Green, 1974), this system shows no evidence of a phase transition to an ordered phase.

With only 5 % dilution on one sublattice (denoted sublattice A), the picture is dramatically different, as shown in Figure 16. The undiluted sublattices, B and C, each show a nonzero magnetization density below a critical temperature of $k_BT/J \approx$

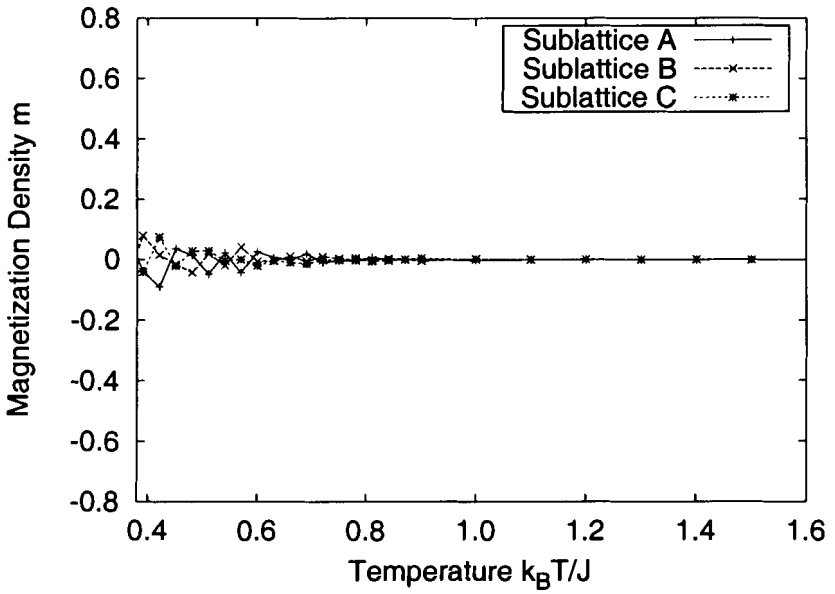

Figure 15: Sublattice magnetization densities m_A, m_B, and m_C vs. temperature k_BT/J for the fully frustrated system. The values were found by averaging over 20,000 measurements taken on a 98×99 lattice.

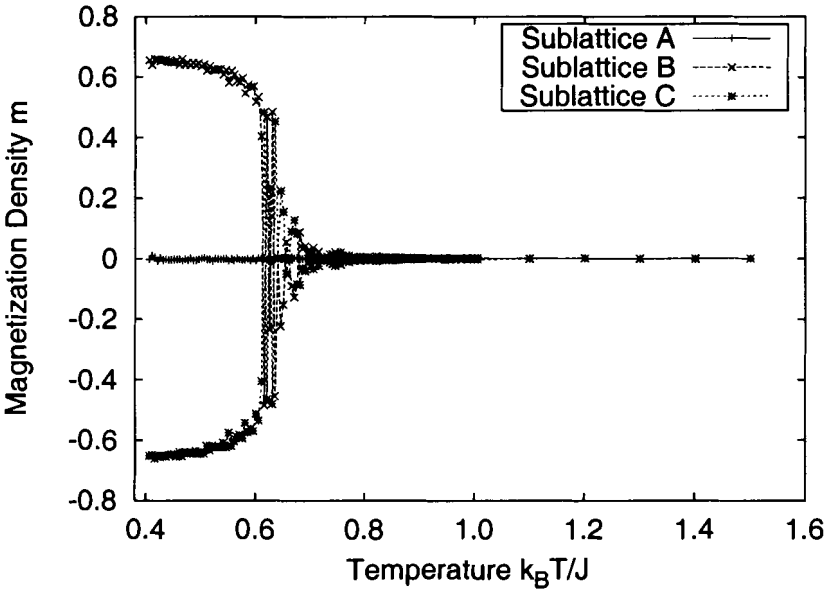

Figure 16: Sublattice magnetization densities m_A, m_B, and m_C vs. temperature k_BT/J for a lattice of 98×99 spins with 5 % of sublattice A randomly diluted. The values were found by averaging over 30,000 measurements.

0.63. The finite size of the lattice causes it to flip over many times near the critical point, making the magnetization data there unreliable. As discussed in Section 4.2.4, we can use the absolute value below the critical temperature when we know what it is. No magnetization density develops on sublattice A, and the whole lattice has no net magnetization. The magnetization densities on sublattices B and C are equal in magnitude but opposite in direction.

Figure 17 shows the effect of dilution on the magnetization density. Two aspects of these results are noteworthy. First, both the maximum sublattice magnetization density and the critical temperature increase as the dilution is increased. Second, the results of this plot qualitatively match those Kaya and Berker obtained via hard-spin mean-field theory (2000). The data points in Figure 17 on the sublattice magnetization density intercept are the result of the analysis of the magnetization critical exponent β discussed below. The line in the 5 % case is a Bézier fit to the data. The other lines are linear interpolations between data points marked by $\times$'s.

Figure 18 illustrates the low-temperature behavior of the magnetization density as a function of dilution. The lines are linear interpolations between the data points marked by the $\times$'s. The change in magnetization density with dilution is largest at low dilutions, providing a very sensitive probe of dilution within this range. By 50 % dilution, the magnetization density has reached 97 % of its magnetization, indicating that the system is reaching saturation.

We have also estimated the magnetization critical exponent β for our system. The magnetization critical exponent β, defined as follows

$$m \sim |T - T_c|^{\beta}, \tag{35}$$

is estimated using a least squares fit of the log of the magnetization versus the log of the deviation of the temperature from the critical temperature.

Our estimates for β are consistent with $\frac{1}{8}$, the exact value for the two-dimensional Ising universality class. By assuming these models have $\beta = \frac{1}{8}$ we can vary T_c until

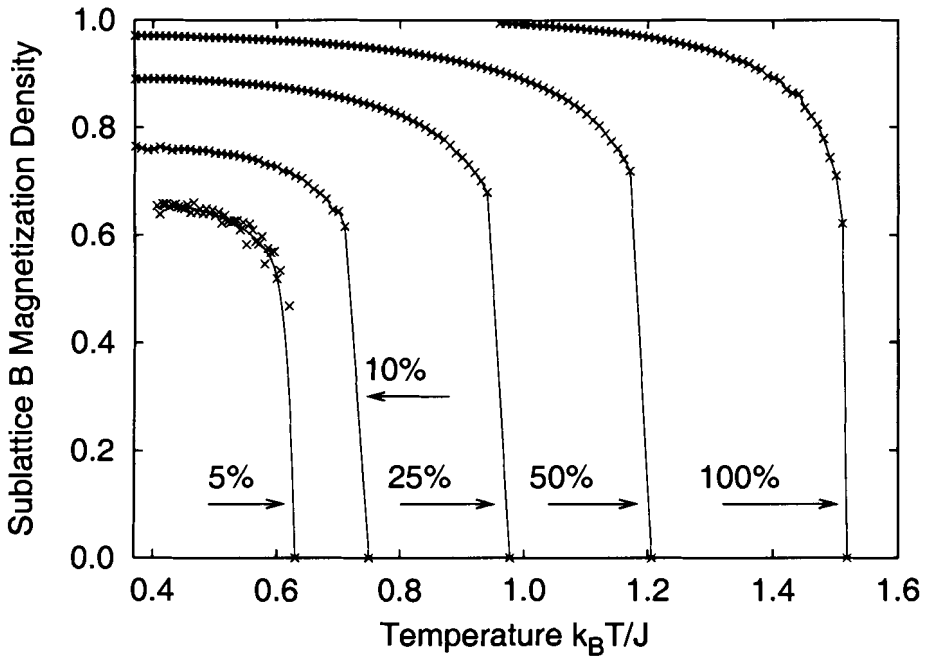

Figure 17: Magnetization density of sublattice B m_B vs. temperature k_BT/J for dilutions of 5%, 10%, 25%, 50%, and 100%. These curves were measured on a 98×99 lattice and came from the average of 30,000 measurements. The data points on the sublattice magnetization density intercept are the result of the analysis of the magnetization critical exponent β. We used a Bézier curve to estimate the 5% diluted data. The other lines are linear interpolations between data points marked by $\times$'s.

the β for our data matches this value and call this the critical temperature of the system. In Figures 19 and 20 only data to the left of the short line crossing the curve was used for the fit. For dilutions close to saturation, the data is very well behaved (e.g. Figure 19), but for low dilutions, the magnetization density fluctuates (e.g. Figure 20) and the slope is less accurate resulting in less accurate identification of the critical exponent. The points on the temperature intercept in Figure 17 were found via this method.

Next we consider the behavior of the Edwards-Anderson order parameter on sublattice A. As stated earlier, this model displays a two-dimensional Ising spin-glass transition at finite temperature. Figure 21 shows the Edwards-Anderson order parameter on sublattice A as a function of temperature. These results were found by

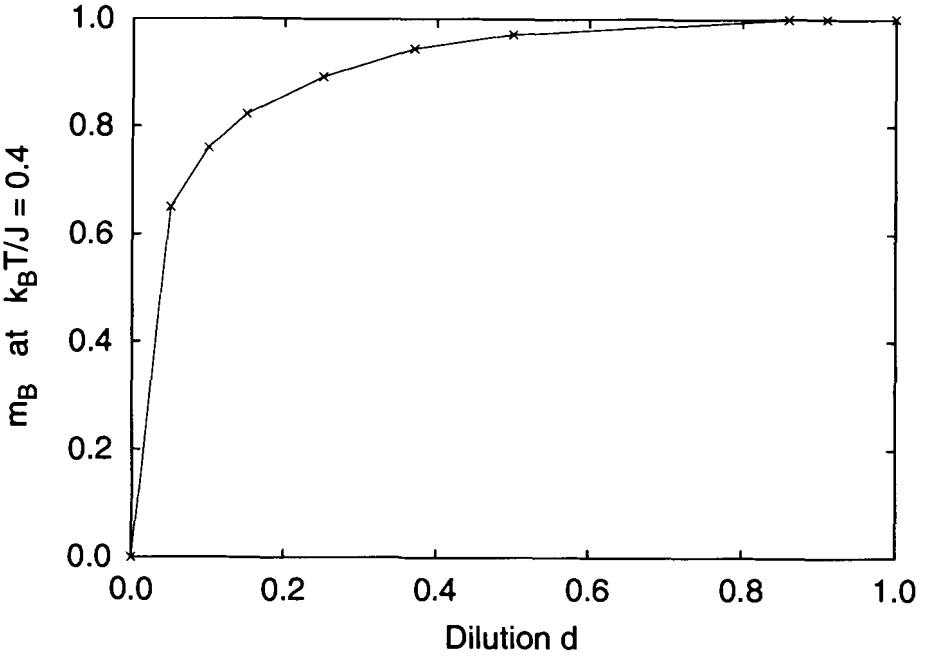

Figure 18: Magnetization density of sublattice B at low temperature vs. dilution. Each data point was obtained via a simulation on a 98×99 lattice at $k_BT/J = 0.4$ and includes an average over at least $25,000$ measurements. The lines are linear interpolations between the data points marked by the $\times$'s.

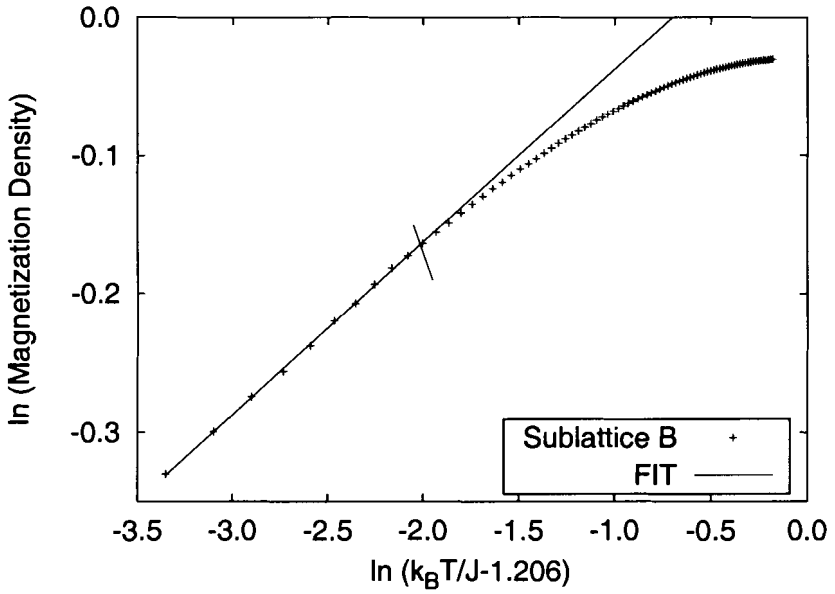

Figure 19: Log of magnetization density vs. log of deviation from critical temperature for 50 % of sublattice A randomly diluted. The data was taken for a lattice of 98×99 spins. The values were found by averaging 30,000 measurements. Only data to the left of the short line crossing the curve was used for the fit. The theoretical value is $\frac{1}{8}$ while the slope of the fitted line is 0.125 ± 0.001.

averaging over $80,000\,MCS$ and the 90.6 % curve is itself an average of six different dynamical pathways. The behaviors at high and low dilutions are qualitatively different. These results agree qualitatively with the hard spin mean field theory (HSMFT) results (Kaya and Berker, 2000); both studies find that the critical temperature values get larger with dilution. In general, HSMFT yields smaller values of the Edwards-Anderson order parameter than our simulations. For example, Kaya and Berker's HSMFT calculation for the 50.0 % diluted case results in a low-temperature limit for q_A of about 0.041, whereas this study shows $q_A \approx 0.068$ for this system. HSMFT shows double reentrance of the Edwards-Anderson order parameter (as temperature is lowered, q_A increases, then decreases, and increases again) for the dilutions calculated above 50.0 %, while our Monte Carlo results do not possess that feature.

As with all results in this thesis, $20\,MCS$ were done between each measurement. The five lower dilution curves look relatively smooth and they were calculated by

averaging over 50,000 measurements. The two higher dilution curves on the other hand, 85.9%, and 90.6%, were averaged over 80,000 MCS measurements, and they are still not smooth. As the number of sites in Sublattice A vanishes, it becomes increasingly difficult to get reliable results for q_A. Further, when we tried to collect data much below $k_BT/J = 0.4$, the q_A data jumps to a value and remains constant. Different simulations produced different values with no correlation with the number of measurements performed thus indicating the minimum temperature accessible by this technique.

Another indication of the phase transition is the structure of the probability distributions used in the information theoretic method. Figure 22 shows a probability distribution above the critical temperature. It is symmetrical because the right hand

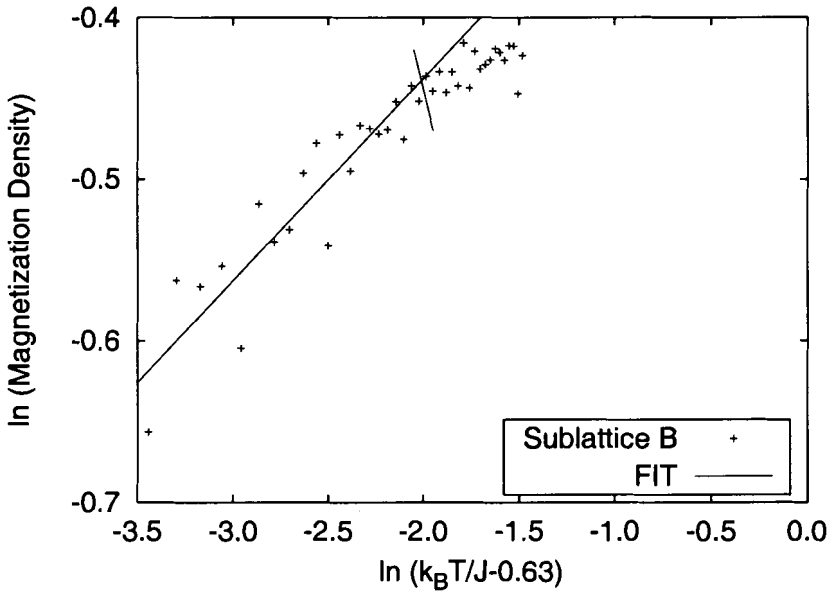

Figure 20: Log of magnetization density vs. log of deviation from critical temperature for 5% of sublattice A randomly diluted. The data was taken on a lattice of 98 × 99 spins. The values were found by averaging 30,000 measurements. Only data to the left of the short line crossing the curve was used for the fit. The theoretical value is $\frac{1}{8}$ while the slope of the fitted line is 0.13 ± 0.01.

side represents configurations connected to the left hand side by spin inversion, reflecting the spin–flip symmetry of the system above its critical temperature. When the lattice goes below a threshold temperature, the local spin–flip symmetry is broken. Figure 23 shows the broken symmetry among the three sublattices. We see a very strong likelihood that the spins will align in just twelve configurations. The histograms reveal a very narrow band of temperatures above which the histograms are symmetric, below which they are not.

Figure 23 shows sets of peaks that have the same ratio of probability between the members in the set. To be explicit, let the triplet just above the 2×3^8 configuration be triplet I, the triplet just above the 6×3^8 configuration be triplet II, and the triplet just above the 8×3^8 configuration be triplet III. Then triplet I differs from triplet III, only in that the spin in the tenth position is flipped. Further, the difference

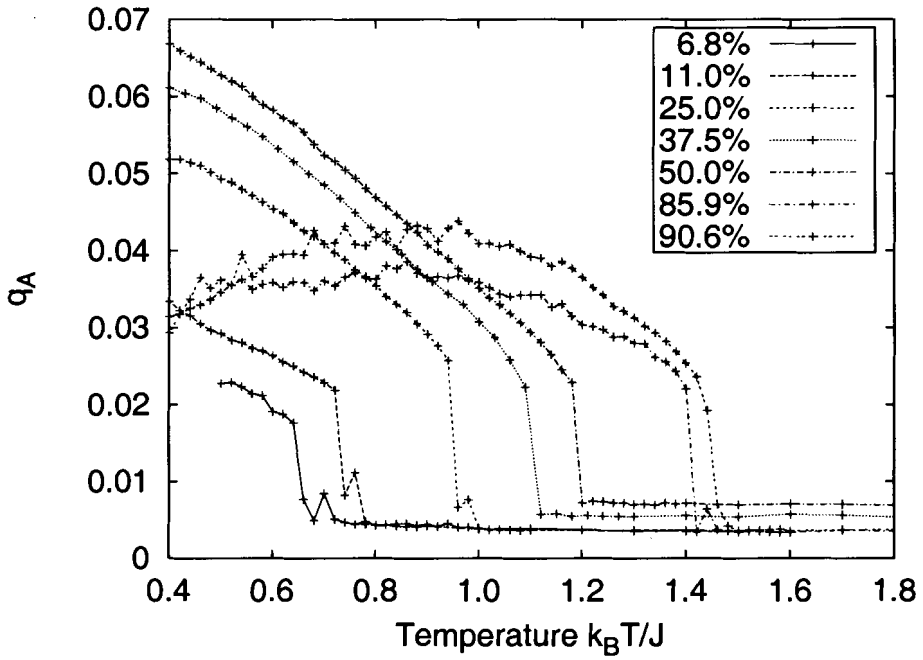

Figure 21: Edwards-Anderson order parameter of sublattice A q_A vs. temperature k_BT/J. Shown are the dilutions in Kaya and Berker : 6.8%, 11.0%, 25.0%, 37.5%, 50.0%, 85.9%, and 90.6 %. All curves were measured on a 98×99 lattice with at least 50,000 measurements. The 85.9 % and 90.6 % curves were averaged over 80,000 measurements.

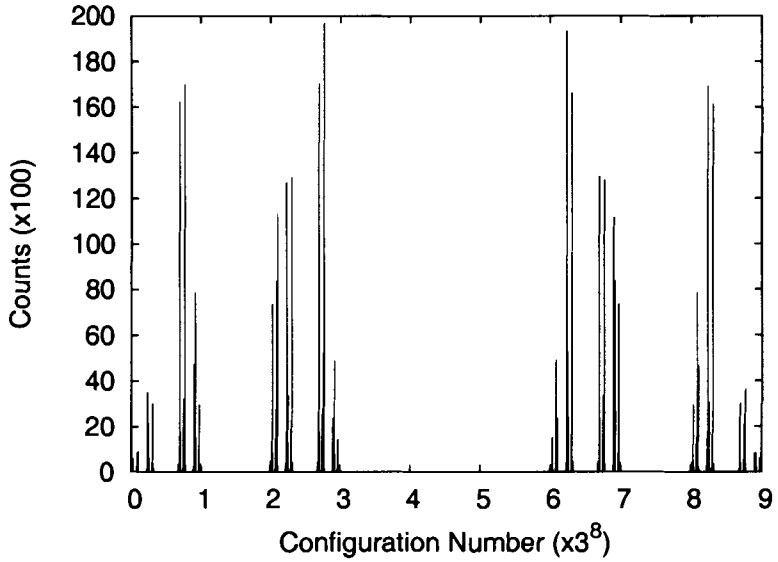

Figure 22: A histogram of 500,000 measurements of a shape in a lattice that has 15% of sublattice A removed at $k_BT/J = 1.0$. $k_BT/J = 1.0$ is above the critical temperature for this system.

between triplet III and triplet II is the flipping of the spin in the ninth position. We see that triplet II differs in form from the other two in that the ratio of the second

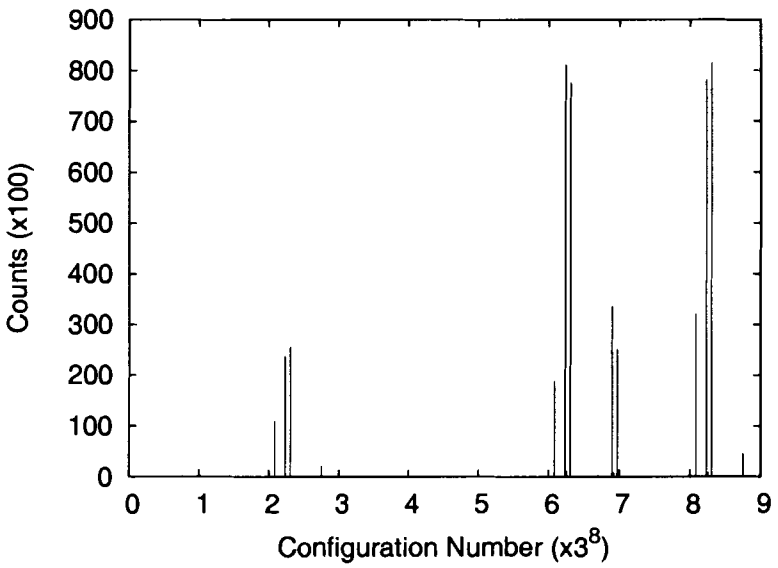

Figure 23: A histogram of 500,000 measurements of a shape in a lattice that has 15% of sublattice A removed at $k_BT/J = 0.5$. $k_BT/J = 0.5$ is below the critical temperature for this system.

peak to the third is the inverse of that ratio for the other two. This shows the effect of the ninth spin on the rest when they are in their lowest energy configurations. What the reader must take away from this discussion is that these low temperature histograms provide insight into which configurations are favorable.

5.2 Comparison of information theoretic results with those of other methods

This study is, to our knowledge, the first time that the information theoretic method for calculating the entropy density has been applied to a system without translational invariance. Although the ensemble of systems studied is translationally invariant, each realization of vacancies is not. As a test of this method, we compared it against various exact results and the results provided by the implementation of the integral method (Section 4.3.1). The Ising model of a ferromagnet on a triangular lattice has no degeneracy of the ground state. All the spins align and the entropy vanishes at $k_BT/J = 0$. It has a well defined phase transition known exactly to occur at $k_BT/J = 3.6410$ (Domb and Green, 1974). The specific heat diverges at the critical temperature so the integral must be performed in two pieces: toward the critical temperature from both sides. Results of this integration and the information theoretic method are compared in Figure 24. Each of the sets of data were obtained from a single run. The agreement between the two methods is excellent.

For the undiluted antiferromagnet there is no finite temperature phase transition so only one integral needs to be performed. The solid line in Figure 25 is the result of this calculation. For comparison, the values found by the implementation of the information theory technique are shown. These values are averages over 20 different runs. Errorbars, given by the standard deviation, do not show since they are smaller than the data points.

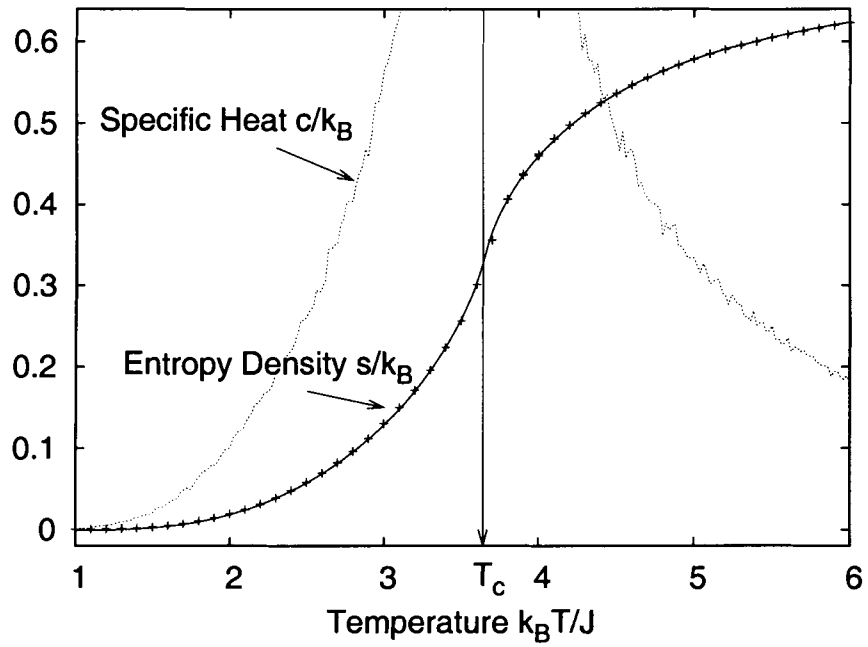

Figure 24: Entropy density s/k_B and specific heat c/k_B vs. temperature k_BT/J for the ferromagnet on a triangular lattice of size 98×99. A correlation time of $50\,MCS$ was used for all measurements. The line was found by integrating under the specific heat data which was collected at intervals of $\Delta k_BT/J = 0.02$. The points were found via the information theoretic method using the sweeping method with $\approx 5\text{x}10^7$ measurements.

These two comparisons verify the equivalence of the two methods for a pure system. Now we test the approach for a system with quenched randomness using the planting method discussed in Section 4.3.2. Figure 26 shows the entropy density s/k_B and specific heat c/k_B as a function of temperature k_BT/J for the 10 % diluted case. The line was found by integrating under the specific heat data (the dotted curve in Figure 26). The points were found via the information theoretic method. In spite of the noise in the specific heat, the integral from high temperature does agree with the information theoretic results. The errorbars were calculated by running the simulation 20 times and calculating the standard deviation. The size of the error bars ($\approx 1\,\%$) are consistent with the expected value that comes from an average of 18,000 local contributors.

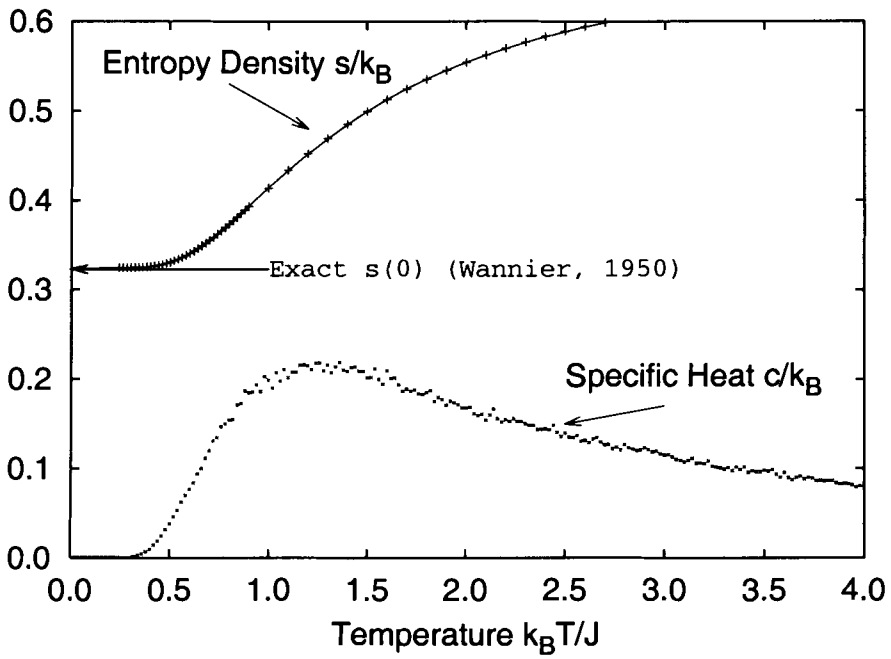

Figure 25: Entropy density s/k_B and specific heat c/k_B vs. temperature k_BT/J for the undiluted antiferromagnet. The measurements were done on a 98 × 99 lattice with a correlation time of 20 MCS. The line was found by integrating under the specific heat data which were collected at intervals of $\Delta k_BT/J = 0.02$. The points were found via the information theoretic method using the sweeping method with $\approx 5\text{x}10^7$ measurements. Both methods agree with the exact zero-temperature result of $s(0) = 0.323066\ k_B$ (Wannier, 1950). The errorbars on the information theoretic method are smaller than the points.

In the specific heat curve in Figure 27 we see the emergence of a little spike (pointed to by the arrow). A feature of this model is that for non-vanishing dilutions below about 25% there are two local maxima in the specific heat.

The entropy curves in Figures 25 and 26 are compared with each other and those of systems with sublattice A dilution of 5%, 15%, 25%, 50%, 95%, and 100% in Figure 28. For the undiluted case, the residual entropy is 0.323066 k_B (Wannier, 1950) and, for the honeycomb lattice ($d = 1.00$), it vanishes. The lines were found by the integration method. The points with errorbars are the results of the information theoretic method. The integral method for the higher dilution is not included as the

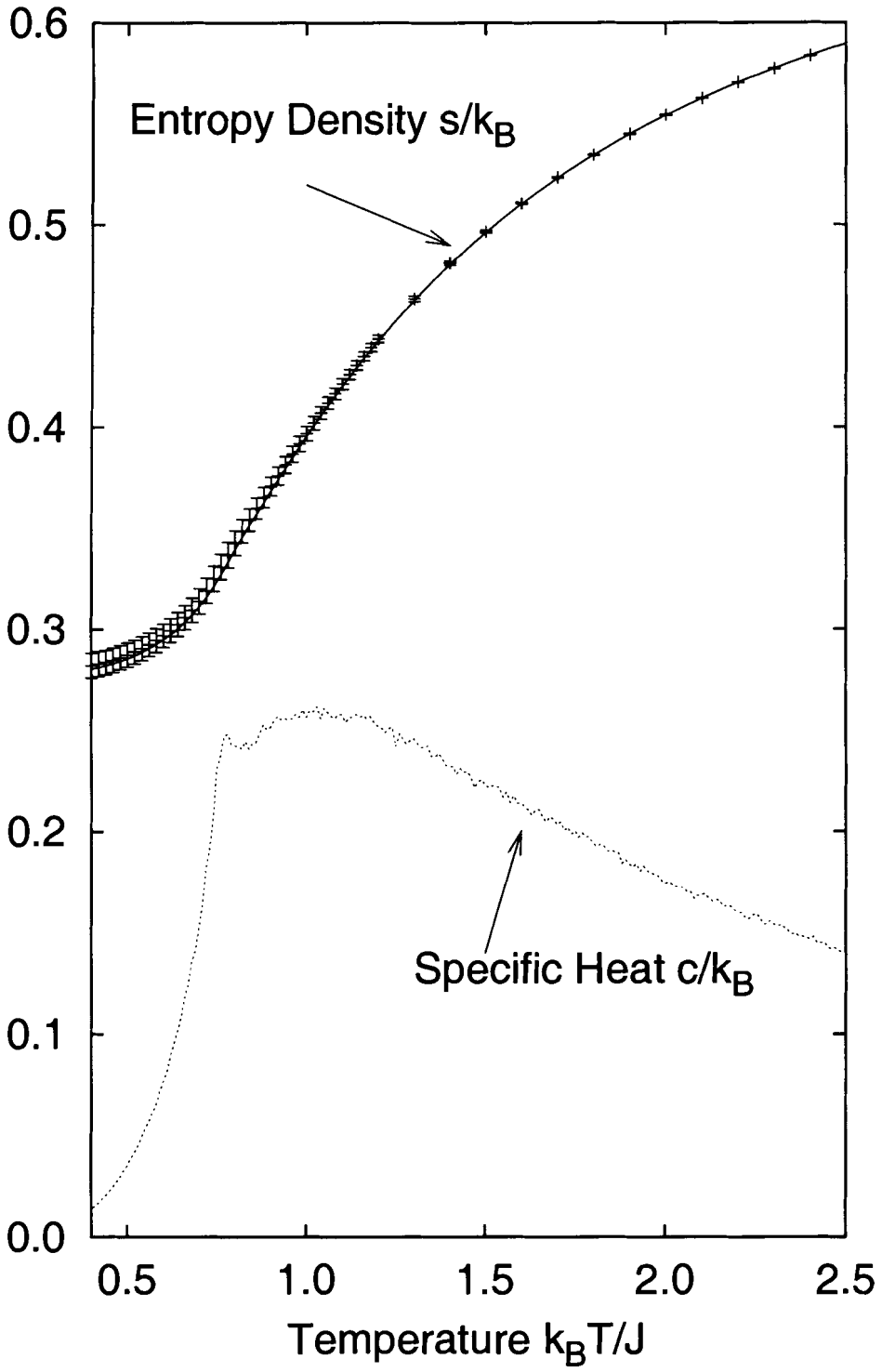

Figure 26: Entropy density s/k_B and specific heat c/k_B vs. temperature k_BT/J for sublattice A diluted 10%. The data was taken on a lattice of size 98×99 and a correlation time of $20\,MCS$ was used between all measurements. The line was found by integrating under the specific heat data which were collected at intervals of $\Delta k_BT/J = 0.02$. The points were found via the information theoretic method with $500,000$ measurements.

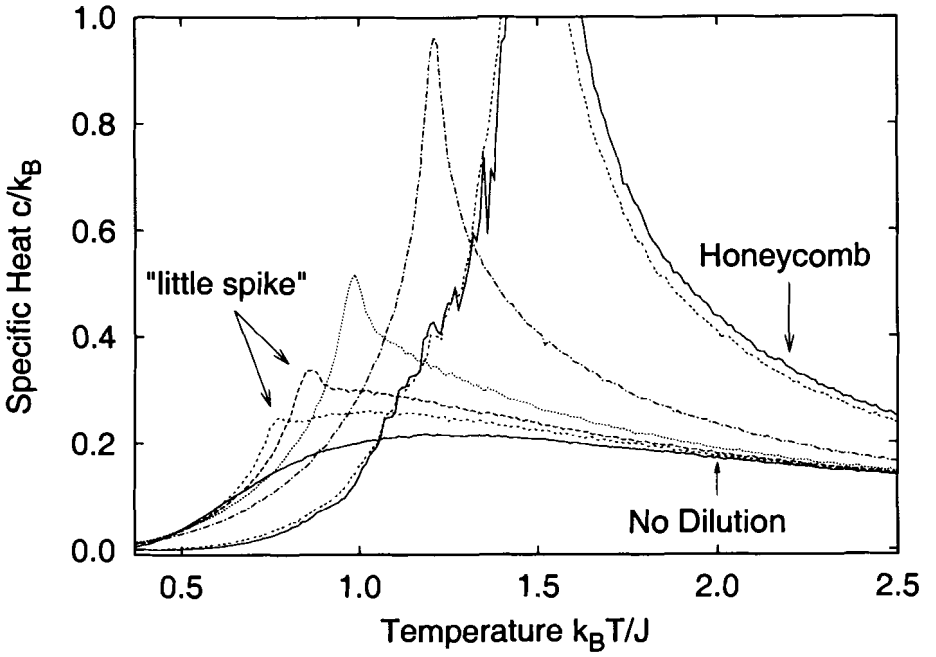

Figure 27: Specific heat c/k_B vs. temperature k_BT/J for a lattice of 98 × 99 spins with dilutions of sublattice A of 0%, 5%, 10%, 15%, 25%, 50%, 95%, and 100%. A correlation time of $20\,MCS$ was used between all measurements, at intervals of $\Delta k_BT/J = 0.02$. We note the origin of the divergence in the specific heat as dilution is increased to $d = 100\%$ by the "little spike" (see text for discussion).

specific heat curve diverges around the critical temperature and the low temperature limit of the entropy is not known exactly.

At low temperatures, this Monte Carlo simulation shows some error due to glassy behavior of the frustrated system as discussed in Sections 4.2 and 5.1. Although Monte Carlo methods do not provide the residual entropy exactly, our results show that our estimates for the residual entropy drop off faster than linearly from the value of Wannier to zero as dilution is increased. This feature can be seen in Figure 29, a plot of the entropy at the lowest reliable temperature vs. dilution. The lowest reliable temperature was between 0.36 and 0.40 depending on dilution. Our estimates are thus an upper bound for the residual entropy. In Figure 29 we see that the residual entropy clearly drops off faster than the linear approximation in the limit of zero dilution. In the undiluted system, the residual entropy drops as a function of dilution as one third

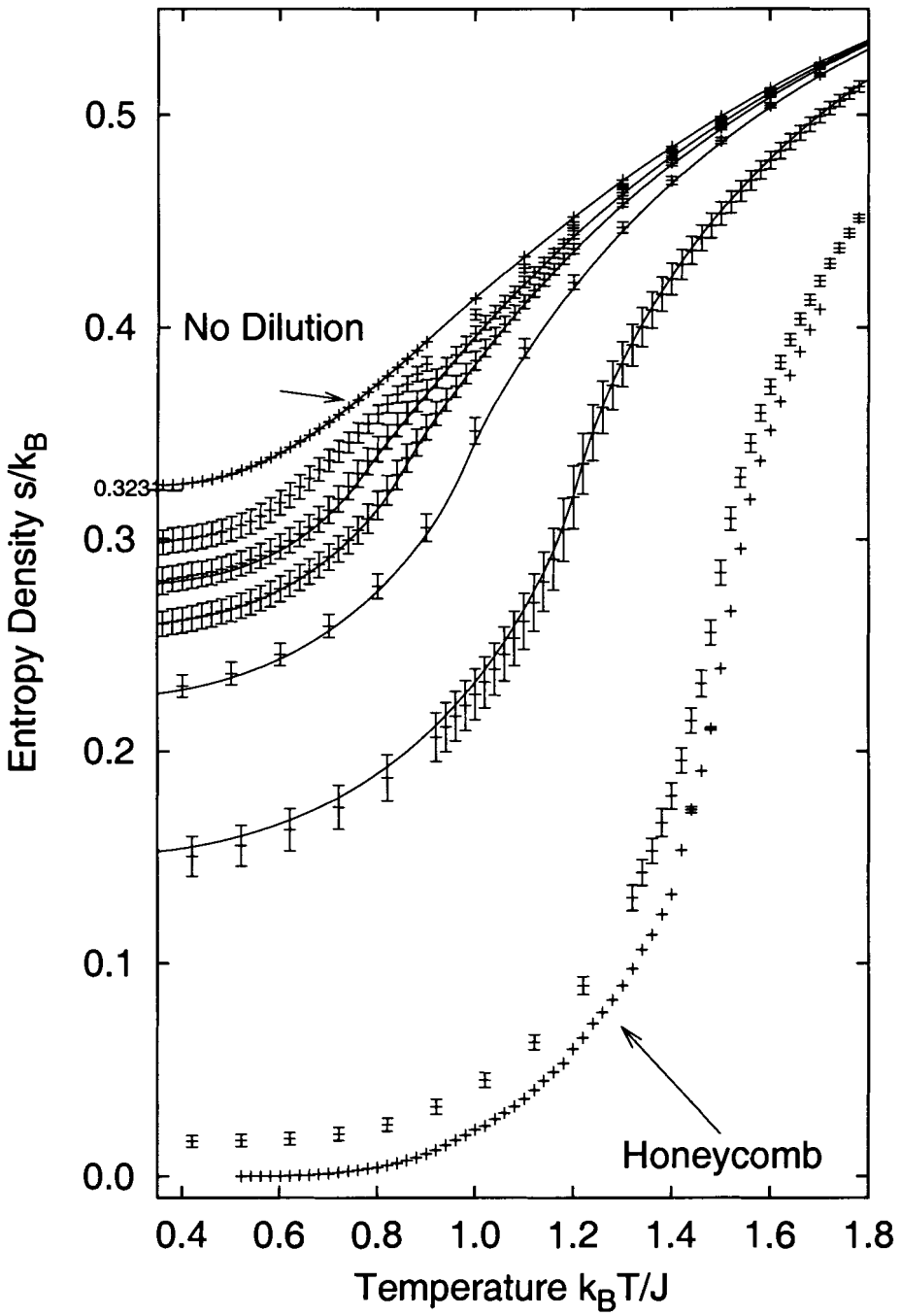

Figure 28: Entropy density s/k_B vs. temperature k_BT/J for a lattice of 98×99 spins with dilutions of sublattice A of 0%, 5%, 10%, 15%, 25%, 50%, 95%, and 100%. A correlation time of $20\,MCS$ was used between all measurements. The lines were found by the integration method using intervals of $\Delta k_BT/J = 0.02$. The points with errorbars were found via the information theoretic method with 20 independent runs of 500,000 measurements each. The integral method for the higher dilution is not included as the specific heat curve is noisy around the critical temperature and so on the lower temperature side of the transition we cannot get meaningful data.

of Farach et al.'s result ($\frac{1}{3} \times 1.9309\, k_B = 0.6436\, k_B$) shown in Figure 29 as the tangent to the curve at the zero dilution limit (Farach et al., 1988; Gonçalves et al., 1997, see Section 2.2).

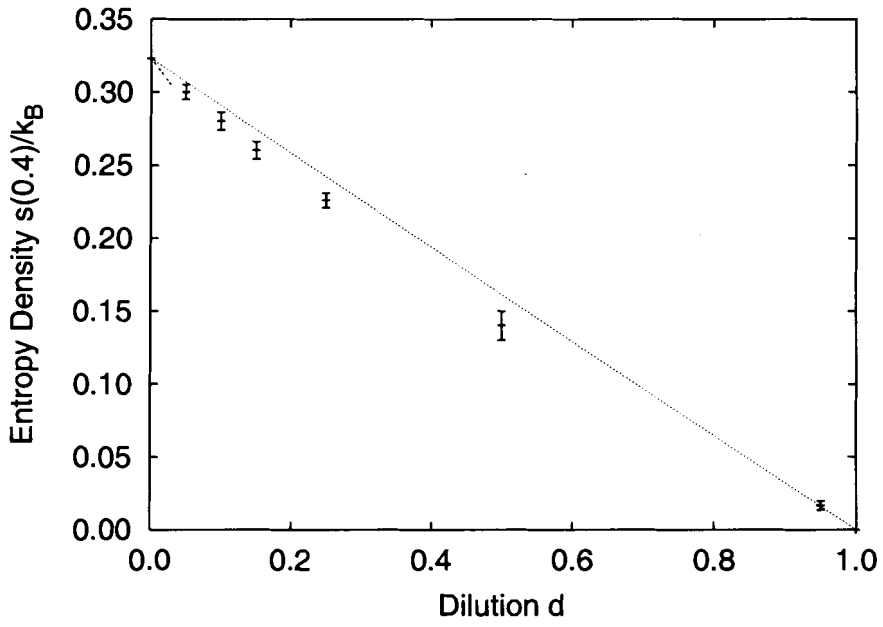

Figure 29: Entropy density at low-temperature vs. dilution. Farach et al.'s calculated slope at zero dilution is represented by a short line segment (see text for details). The simulations were done on 98×99 lattice with a correlation time of $20\, MCS$ between all measurements and $500,000$ measurements contributed to the histograms. The errorbars represent the standard deviation of 18,000 local contributions.

5.3 Local contributions to the entropy density

For systems that are spatially homogeneous, the individual local contributions to the information theoretic calculation of the entropy density lie very close to each other. By local contributions, we mean the value of the entropy density at a single site, arrived at via the planted method, discussed in Section 4.3.2. In Figure 30 a set of 67 local entropy contributions is displayed for a run on the undiluted antiferromagnet. Recall that for the planted method the entropy calculation is made by taking an average over many individual local entropy contributions (see Section 4.3.2).

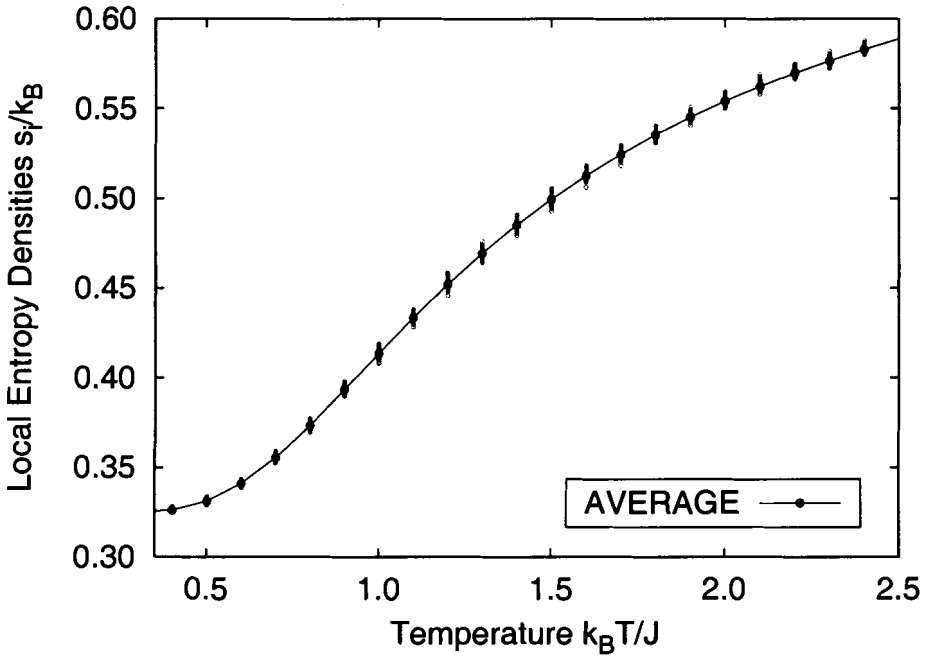

Figure 30: A sample of 67 local entropy densities s_i/k_B and the mean of all 900 vs. temperature k_BT/J for the undiluted lattice. The data was collected on a lattice of size 98×99. A correlation time of $20\,MCS$ was used and there were $500,000$ measurements contributing to the average.

When random quenched dilution is introduced the local contributions are no longer identical and the position of the shape in the lattice becomes important. Figures 31-36 show the cases of sublattice A diluted 5 %, 10 %, 15 %, 50 %, 95 %, and 100 % respectively. Each local entropy density has a high temperature value of $k_B \ln(2)$, but as the temperature is lowered the local entropy densities become spatially inhomogeneous. With only 5 % dilution, the local contributions have a large spread. Many of the sites undergo reentrance – the entropy density actually rises as temperature decreases beyond a certain temperature. The spins which undergo reentrance at higher temperatures rise to higher low-temperature entropy density while those which undergo reentrance at lower temperatures only rise in entropy density marginally above their lowest value.

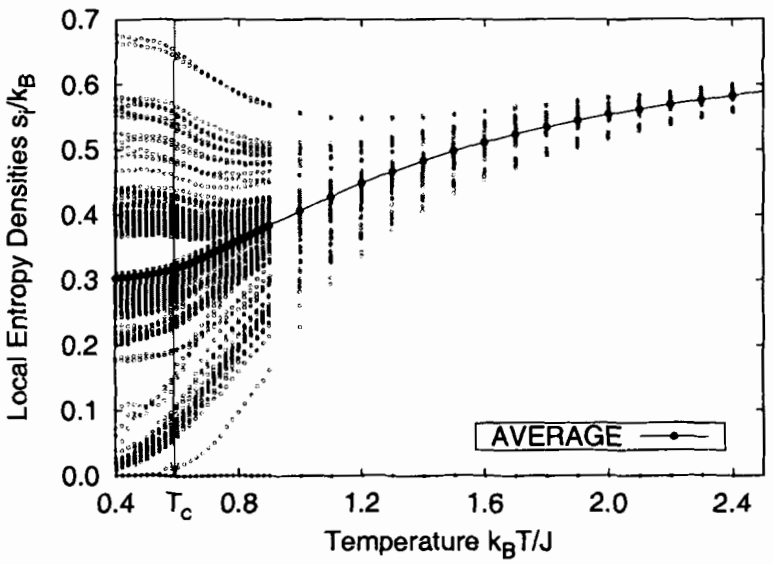

Figure 31: A random sample of 200 local entropy densities s_i/k_B and the mean local entropy density vs. temperature k_BT/J for a 98×99 lattice with 5 % of sublattice A removed. Measurements were taken every $20\,MCS$ and there were $500,000$ measurements contributing to the average. The mean local entropy density was obtained by averaging 900 local entropy densities, not all of which are shown. The local entropy densities spread as the temperature is lowered and we see forbidden regions form. The critical temperature $k_BT/J \approx 0.63$ is indicated by the arrow.

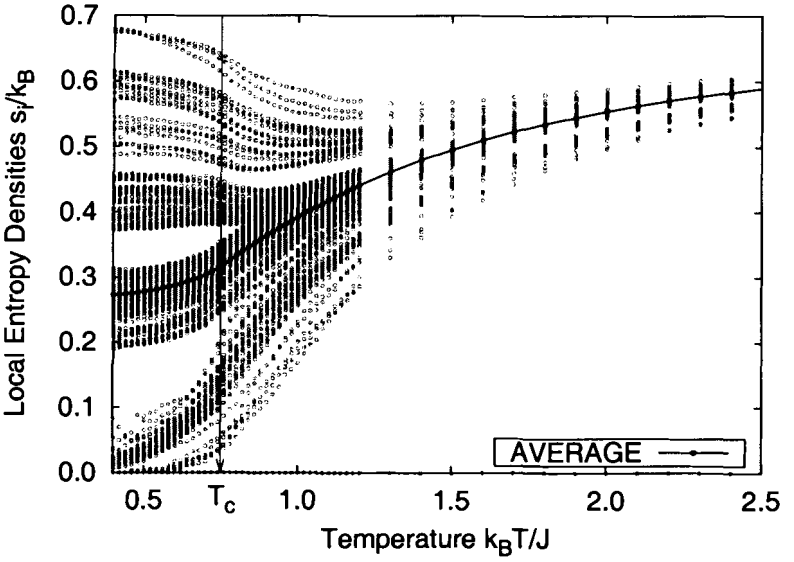

Figure 32: A random sample of 200 local entropy densities s_i/k_B and the mean local entropy density vs. temperature k_BT/J for a 98×99 lattice with 10 % of sublattice A removed. Measurements were taken every 20 MCS and there were 500, 000 measurements contributing to the average. The mean local entropy density was obtained by averaging 900 local entropy densities, not all of which are shown. The local entropy densities spread as the temperature is lowered and we see forbidden regions form. The critical temperature $k_BT/J \approx 0.76$ is indicated by the arrow.

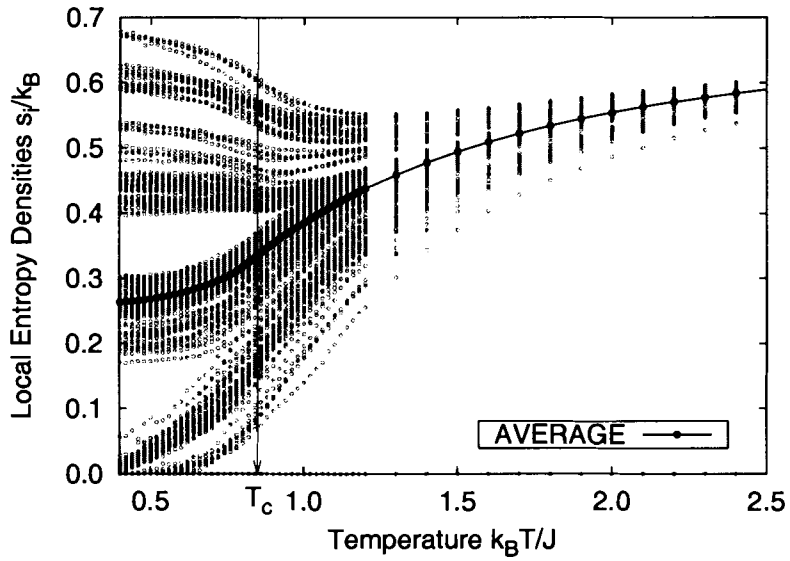

Figure 33: A random sample of 200 local entropy densities s_i/k_B and the mean local entropy density vs. temperature k_BT/J for a 98×99 lattice with 15 % of sublattice A removed. Measurements were taken every 20 MCS and there were 500,000 measurements contributing to the average. The mean local entropy density was obtained by averaging 900 local entropy densities, not all of which are shown. The local entropy densities spread as the temperature is lowered and we see forbidden regions form. The critical temperature $k_BT/J \approx 0.85$ is indicated by the arrow.

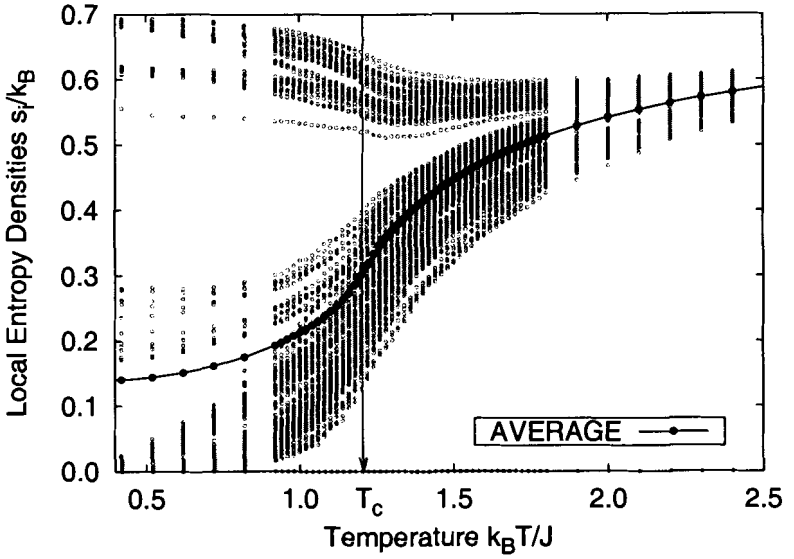

Figure 34: A random sample of 200 local entropy densities s_i/k_B and the mean local entropy density vs. temperature k_BT/J for a 98×99 lattice with 50 % of sublattice A removed. Measurements were taken every 20 MCS and there were 500,000 measurements contributing to the average. The mean local entropy density was obtained by averaging 900 local entropy densities, not all of which are shown. The local entropy densities spread as the temperature is lowered and we see forbidden regions form. The critical temperature $k_BT/J \approx 1.206$ is indicated by the arrow.

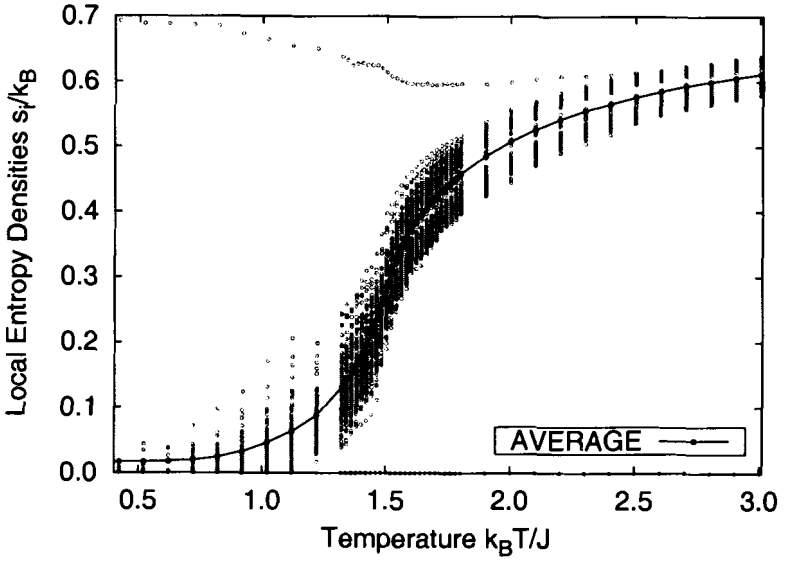

Figure 35: A random sample of 200 local entropy densities s_i/k_B and the mean local entropy density vs. temperature k_BT/J for a 98×99 lattice with 95 % of sublattice A removed. Measurements were taken every $20\,MCS$ and there were $500,000$ measurements contributing to the average. The mean local entropy density was obtained by averaging 900 local entropy densities, not all of which are shown.

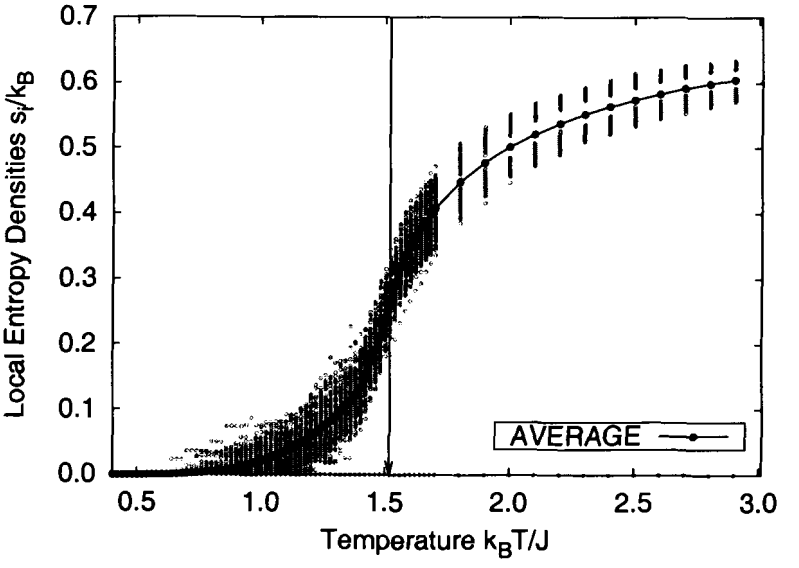

Figure 36: A random sample of 200 local entropy densities s_i/k_B and the mean local entropy density vs. temperature k_BT/J for a 98×99 lattice with 100 % of sublattice A removed. Measurements were taken every $20\,MCS$ and there were $500,000$ measurements contributing to the average. The mean local entropy density was obtained averaging 900 local entropy densities, not all of which are shown.

Certain regions of local entropy density at low temperatures are never occupied. A striking feature of these "forbidden regions," due to the reentrance phenomena, is the formation of a *central gap*. As dilution increases, the central gap increases until it reaches its maximum width at $d = 1$. In the 95 % case a small fraction still go up to approximately $k_B \ln 2$ and so we expect the maximum central gap to be this value. In addition to the central gap, some dilutions also show a "fine structure." For example, in the 50 % case one can see at least three gaps besides the central one.

The lower dilutions appear more complex than the higher ones in that the low-temperature limit of the local entropies span extended intervals as opposed to the discrete locations seen for the higher dilutions. In contrast, for large dilutions in the low-temperature limit the local entropies are distributed in very narrow bands.

Figures 37 and 38 show how the high and low local entropy densities are spatially distributed on a 30×30 subset of the lattice for the 15 % diluted case. The vacancies can be identified as the blue "pits" in these entropy landscape plots. Red indicates the regions of highest entropy. In Figure 37, the local entropy densities above the critical temperature show regions of high local entropy density immediately next to the vacancies, while the rest of the lattice is very near a uniform value. The uncertainty of one of the spins near a vacancy, given the state of its neighbors, is relatively large and in some cases near $k_B \ln(2)$ (see Figure 33). Some of the spins have yet to undergo reentrance so we expect to see more red at lower temperatures.

Figure 38 shows the local contributors below the critical temperature. Here we see bands of spins with high entropy density between bands of lower entropy density. The spins in areas of high entropy density are on sublattice A which is indicated by the fact that all the vacancies lie on these ridges. The low entropy density bands correspond to the other two sublattices. Given the state of the surrounding spins, there is less uncertainty of the orientation of a spin on the two undiluted sublattices than that of the orientation of a spin on sublattice A.

Figure 37: A sample 30×30 block of local entropy densities s_i/k_B at temperature $k_BT/J = 1.0$ with 15 % of sublattice A removed. A correlation time of $20\,MCS$ was used and there were $500,000$ measurements contributing to the average.

The spread of local entropy contributions shown in Figures 31-36 as a function of temperature can be characterized by their standard and relative deviations. The standard deviation of the local entropy densities σ_s is found by the usual formula:

$$\sigma_s(T) = \sqrt{\frac{\sum_{i=1}^{K} (s_i - s(T))^2}{K-1}}, \tag{36}$$

where s_i is one of the K local entropies that go into the calculation and $s(T)$ is the mean of the local entropies. The relative deviation, the unitless ratio of the standard deviation of the local entropies to the entropy itself, $\frac{\sigma_s}{s}$, provides a measure of the spread normalized to the entropy density itself. Figure 39 shows the standard and relative deviations of the local entropy densities for the system that has sublattice A 5 % diluted. The standard deviation rises monotonically from zero as temperature is reduced from infinity, as expected from the plot of the individual local entropy densities. Further, in Figure 39, the relative deviation also monotonically rises from zero as the system is cooled.

Figure 38: A sample 30×30 block of local entropy densities s_i/k_B at temperature $k_BT/J = 0.5$ with 15 % of sublattice A removed. A correlation time of $20\,MCS$ was used and there were $500,000$ measurements contributing to the average.

For some dilutions the standard deviation of the local entropy contributions does not change monotonically. The standard deviations of the local entropy contributions for various dilutions are compared in Figure 40. Here we see the spread of the local entropies grows monotonically as temperature decreases for dilutions above 0 % and below some dilution between 95 % and 100 %. The spread σ_s itself increases for any given temperature from a dilution of 0 % to one greater than 50 %. On first blush it appears as if there is a certain dilution somewhere between 50 % and 95 % that has the maximum spread. Certainly the standard deviation drops as dilution is increased beyond 95 % until it finally takes on the form of the honeycomb limit curve shown in Figure 40.

The relative deviation of the local entropy contributions for various dilutions are compared in Figure 41. Here we see a monotonic growth in the relative deviations. This means that as dilution increases, although the spread goes through some kind

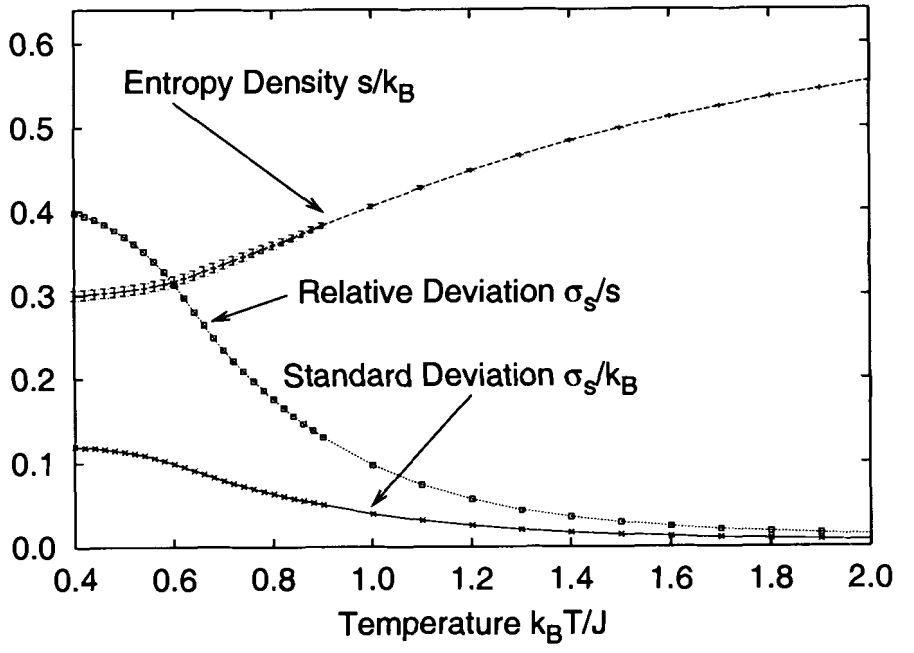

Figure 39: Entropy density s/k_B and the standard and relative deviations of entropy density σ_s/k_B, σ_s/s vs. temperature k_BT/J for a lattice with 5 % of sublattice A randomly diluted. The data were taken on a lattice of size 98×99 and a correlation time of $20\,MCS$ was used between all measurements.

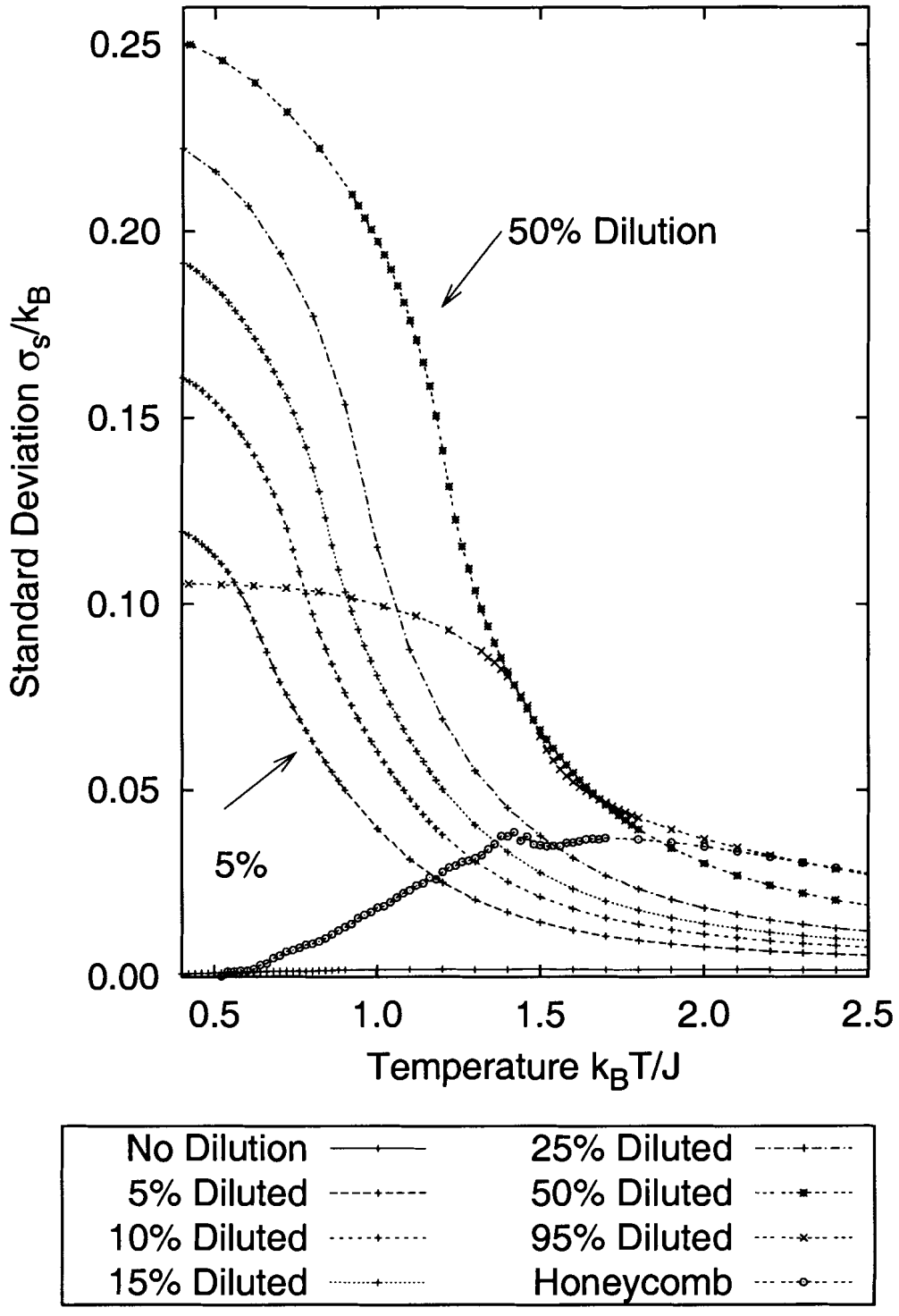

Figure 40: Standard deviation σ_s/k_B vs. temperature k_BT/J for a lattice with various dilutions of sublattice A. Measurements were taken on a lattice of size 98×99 every $20\,MCS$, there were $500,000$ measurements contributing to the average, for each shape, and between 9,000 and 18,000 shapes were used for the calculation of each point. The standard deviation reaches a maximum between dilutions of 25 % and 95 %.

of maximum and then decreases, the ratio of the spread to the actual value always increases.

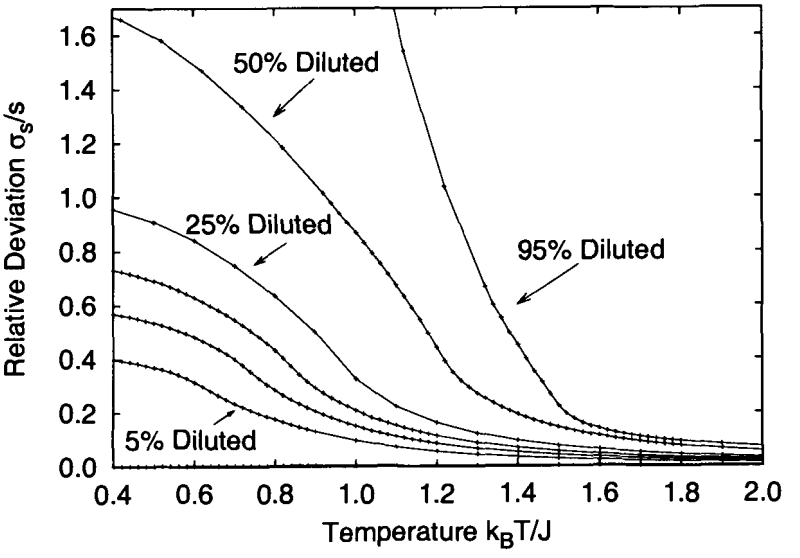

Figure 41: Relative deviation σ_s/s vs. temperature k_BT/J for a 98×99 lattice with 0%, 5%, 10%, 15%, 25%, 50%, and 95% of sublattice A removed. Measurements were taken every 20 MCS, there were 500,000 measurements contributing to the average of each shape, and between 9,000 and 18,000 shapes were used for the calculation of each point.

Finally, we present the residual relative deviation as a function of dilution in Figure 42. It grows approximately linearly as dilution increases from zero to about $d = 0.5$ at which point the residual relative deviation grows much faster.

5.4 Excess entropy

The local contributions to the excess entropy behave in much the same way as those of the entropy density. In Figure 44 we plot the excess entropy vs. temperature for the spatially homogeneous undiluted lattice. Note that the local entropies do not spread out for the undiluted lattice as in Figure 43. The mean excess entropy for the different dilutions is compared in Figure 50. For the systems of nonvanishing dilution studied in this thesis, we see the formation of a cusp in the excess entropy that reaches

its maximum value near the estimate of the critical temperature we found using the magnetization data (see Section 5.1).

In Figures 44-49 we plot the local excess entropies vs. temperature for dilutions of 5%, 10%, 15%, 50%, 95%, and 100%. The spread of these plots can also be characterized by a standard deviation:

$$\sigma_E(T) = \sqrt{\frac{\sum_{i=1}^{K} (E_i - E(T))^2}{K-1}} \tag{37}$$

where E_i is one of the K local excess entropies that go into the calculation and $E(T)$ is the mean of the local excess entropies. The relative deviation, $\frac{\sigma_E}{E}$, is also calculated.

The standard deviation of systems where sublattice A is diluted 0%, 5%, 10%, 15%, 50%, 95%, and 100% are compared in Figure 52. For the cases of low dilution the peak of the cusp is very pronounced, making this a strong indicator of the temperature for which the correlation length has its maximum, the critical temperature. For dilutions greater than 50% the standard deviation is quite low and therefore hard

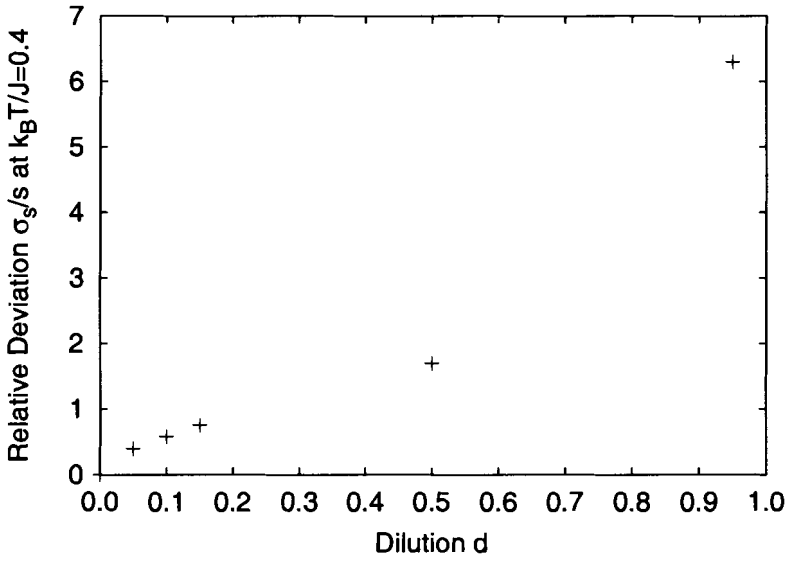

Figure 42: Relative deviation at $k_BT/J = 0.4$ vs. dilution d. The data were taken on a lattice of 98×99 sites with 20 MCS between all measurements, 500,000 measurements contributed to the histograms of each shape, and between 9,000 and 18,000 shapes were used for the calculation of each point.

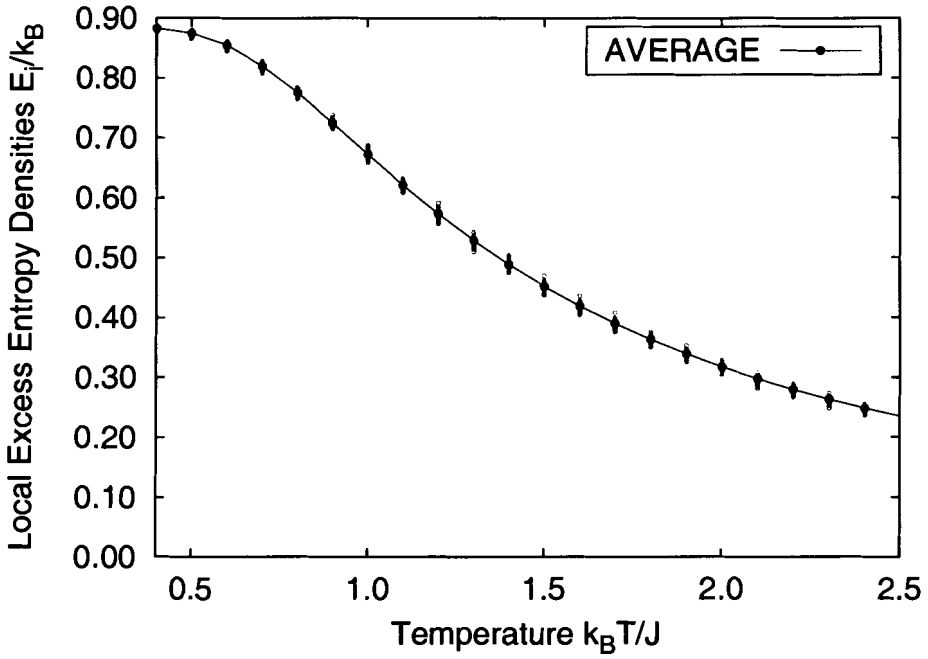

Figure 43: A sample of 67 local excess entropies E_i/k_B and the mean of all 900 vs. temperature k_BT/J for an undiluted lattice. The data were taken on a lattice of size 98×99 and measurements were taken every $20\,MCS$ and there were $500,000$ measurements contributing to the average. The mean was calculated by averaging over 900 local excess entropies, not all of which are shown.

to interpret. The values of the critical temperature found by locating the cusp in the excess entropy are compared against those found via the magnetization density critical exponent (Section 5.1) in Figure 53. The errorbars in Figure 53 are estimated by the coarseness of the temperature step. The critical temperatures given by this estimate agree with those found by the critical exponent method. This suggests that the excess entropy is indeed maximized at the critical temperature.

The relative deviation of systems where sublattice A is diluted 0%, 5%, 10%, 15%, 25%, 50%, 95%, and 100% are compared in Figure 54. Except perhaps for a very small neighborhood of the critical temperatures (where our Monte Carlo simulation is somewhat less reliable) the relative deviation of the local excess entropies increases monotonically as temperature is decreased for nonvanishing dilutions less than some value between 50% and 95%. For the higher dilutions we see reentrance;

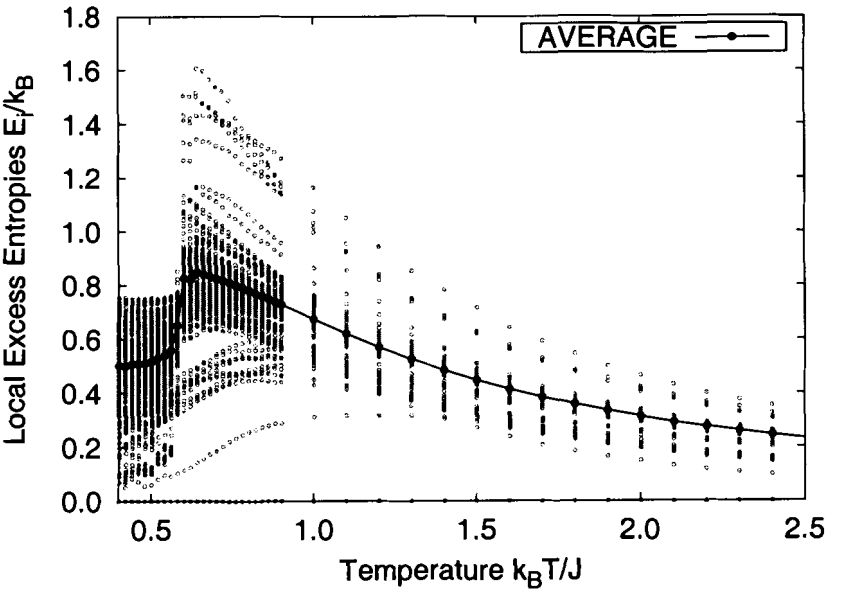

Figure 44: A random sample of 200 local excess entropies E_i/k_B and the mean excess entropy vs. temperature k_BT/J for lattice with 5% of sublattice A removed. The data were taken on a lattice of size 98×99, measurements were taken every $20\,MCS$, and there were $500,000$ measurements contributing to the average. The mean was calculated by averaging over 900 local excess entropies, not all of which are shown.

the relative deviation of local excess entropies decreases as temperature decreases until the critical temperature is reached, at which point they increase.

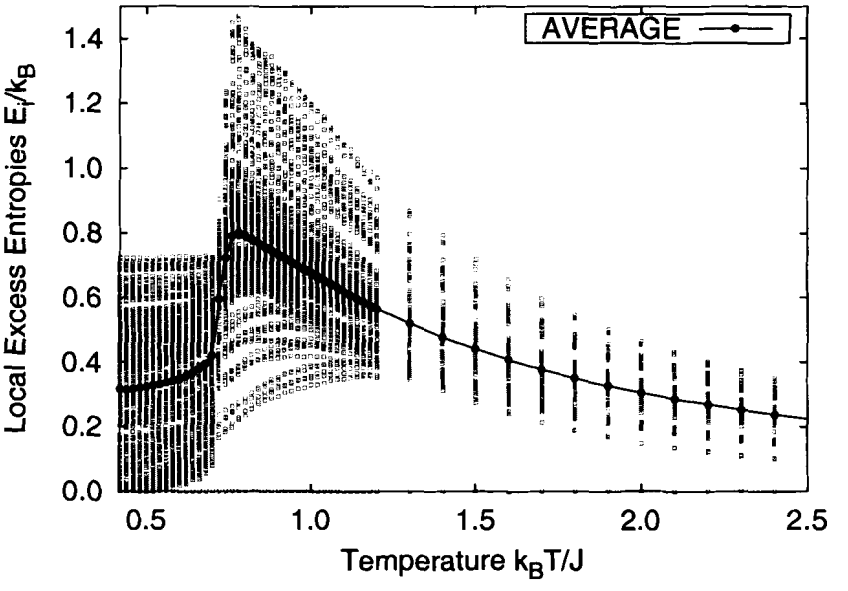

Figure 45: A random sample of 200 local excess entropies E_i/k_B and the mean excess entropy vs. temperature k_BT/J for a lattice with 10 % of sublattice A removed. The data were taken on a lattice of size 98×99, measurements were taken every $20\,MCS$, and there were $500,000$ measurements contributing to the average. The mean was calculated by averaging over 900 local excess entropies, not all of which are shown.

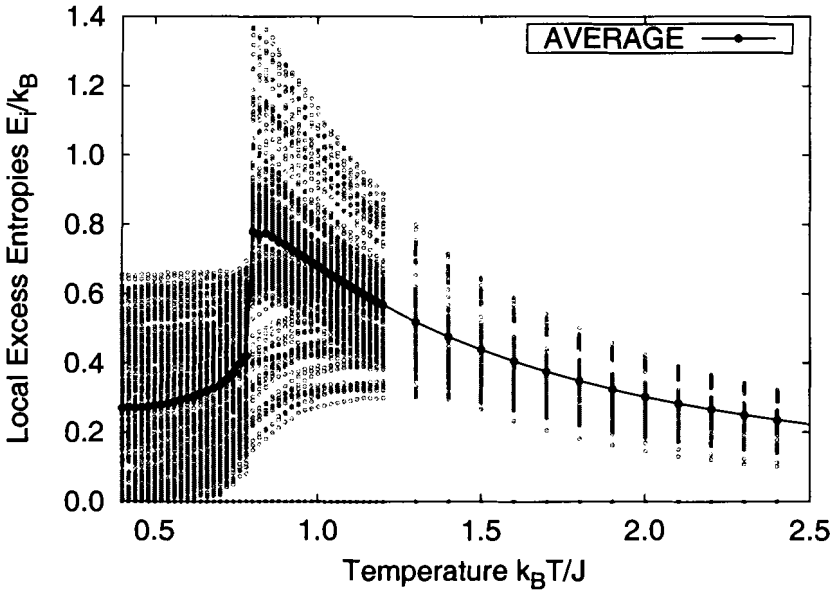

Figure 46: A random sample of 200 local excess entropies E_i/k_B and the mean excess entropy vs. temperature k_BT/J for a lattice with 15 % of sublattice A removed. The data were taken on a lattice of size 98×99, measurements were taken every $20\,MCS$, and there were $500,000$ measurements contributing to the average. The mean was calculated by averaging over 900 local excess entropies, not all of which are shown.

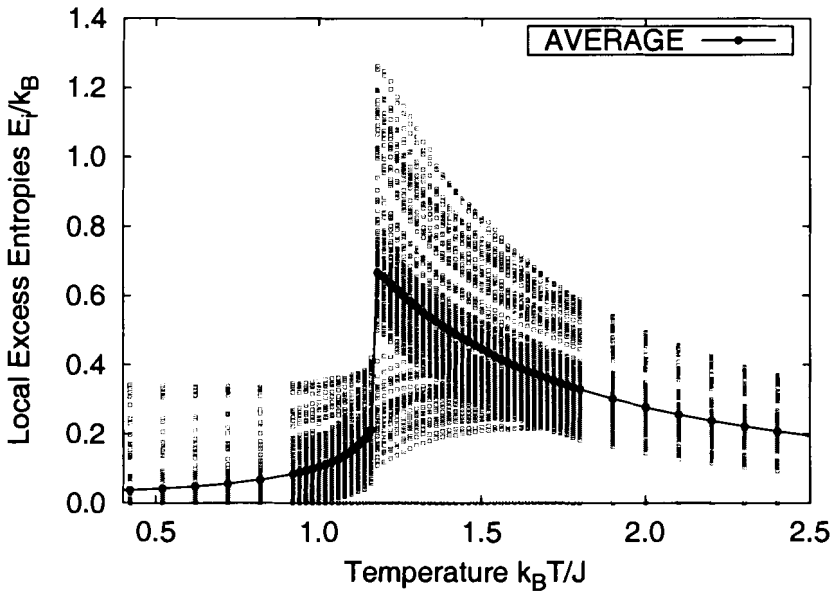

Figure 47: A random sample of 200 local excess entropies E_i/k_B and the mean excess entropy vs. temperature k_BT/J for a lattice with 50 % of sublattice A removed. The data were taken on a lattice of size 98×99, measurements were taken every 20 MCS, and there were 500,000 measurements contributing to the average. The mean was calculated by averaging over 900 local excess entropies, not all of which are shown.

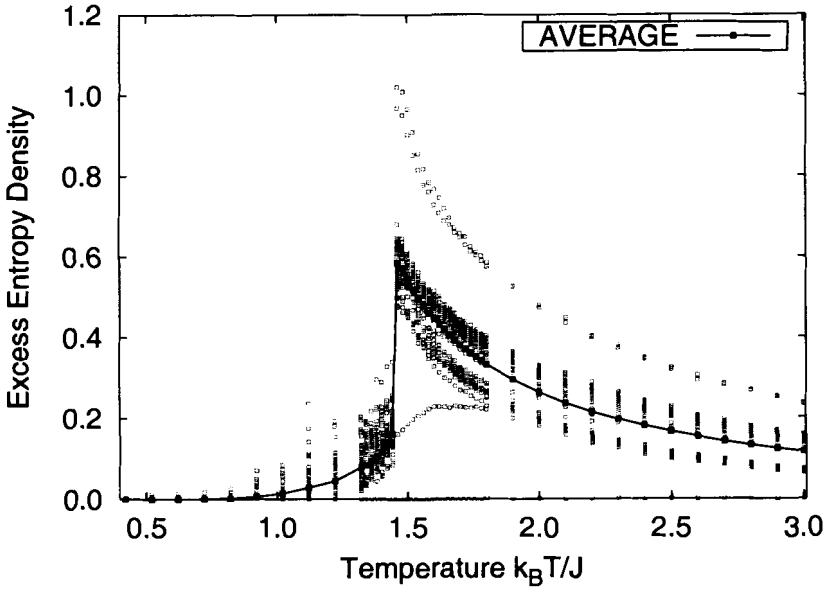

Figure 48: A random sample of 200 local excess entropies E_i/k_B and the mean excess entropy vs. temperature k_BT/J for a lattice with 95 % of sublattice A removed. The data were taken on a lattice of size 98×99, measurements were taken every 20 MCS, and there were 500,000 measurements contributing to the average. The mean was calculated by averaging over 900 local excess entropies, not all of which are shown.

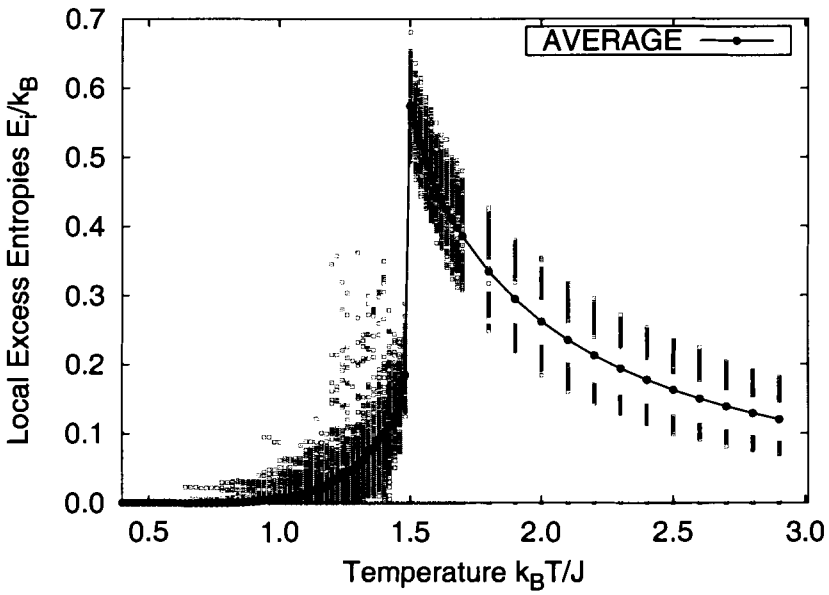

Figure 49: A random sample of 200 local excess entropies E_i/k_B and the mean excess entropy vs. temperature k_BT/J for a lattice with 100% of sublattice A removed. The data were taken on a lattice of size 98×99, measurements were taken every $20\,MCS$, there were $500,000$ measurements contributing to the average. The mean was calculated by averaging over 900 local excess entropies, not all of which are shown.

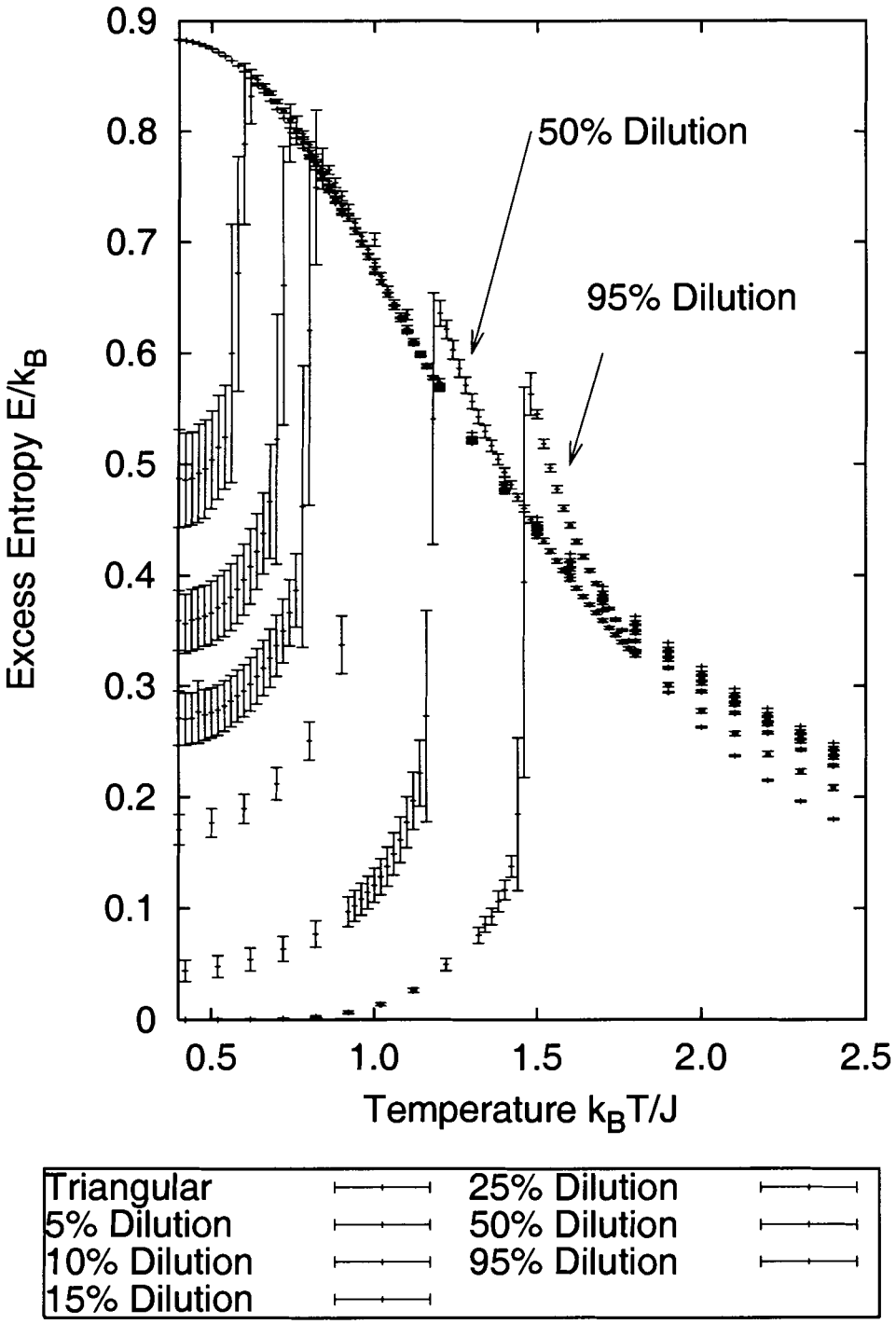

Figure 50: Excess entropy density E/k_B vs temperature k_BT/J for a lattice of 98×99 spins with dilutions of sublattice A of 0%, 5%, 10%, 15%, 25%, 50%, and 95%. Measurements were taken every 20 MCS. The points with errorbars were found by averaging with 20 independent runs of 500,000 measurements each. The errorbars are the standard deviation of the 20 excess entropy values.

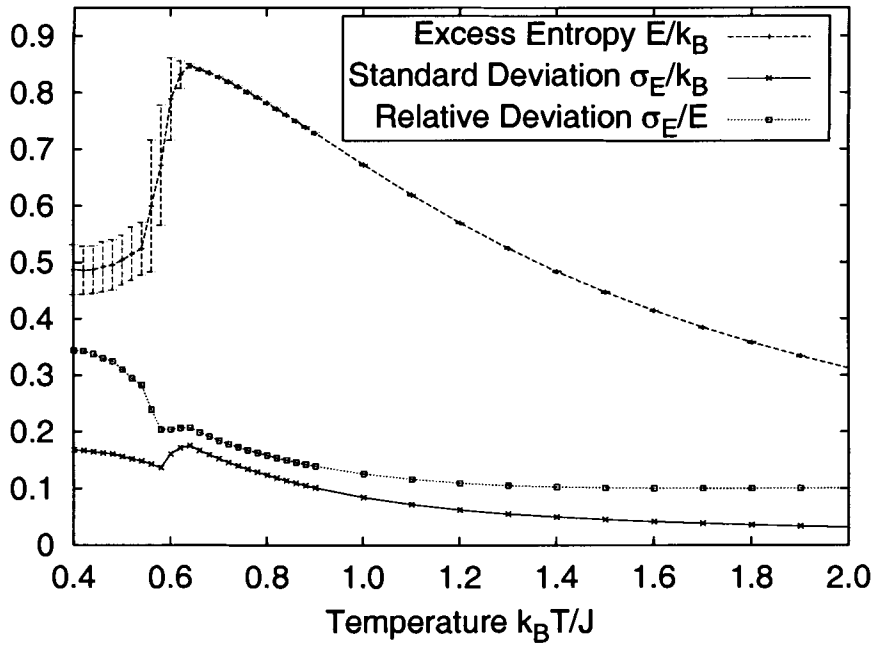

Figure 51: Excess entropy E/k_B and the standard and relative deviations of entropy density σ_E/k_B, σ_E/E vs. temperature k_BT/J for a lattice with 5 % of sublattice A removed. The data was taken on a lattice of size 98×99 and measurements were taken every $20\,MCS$.

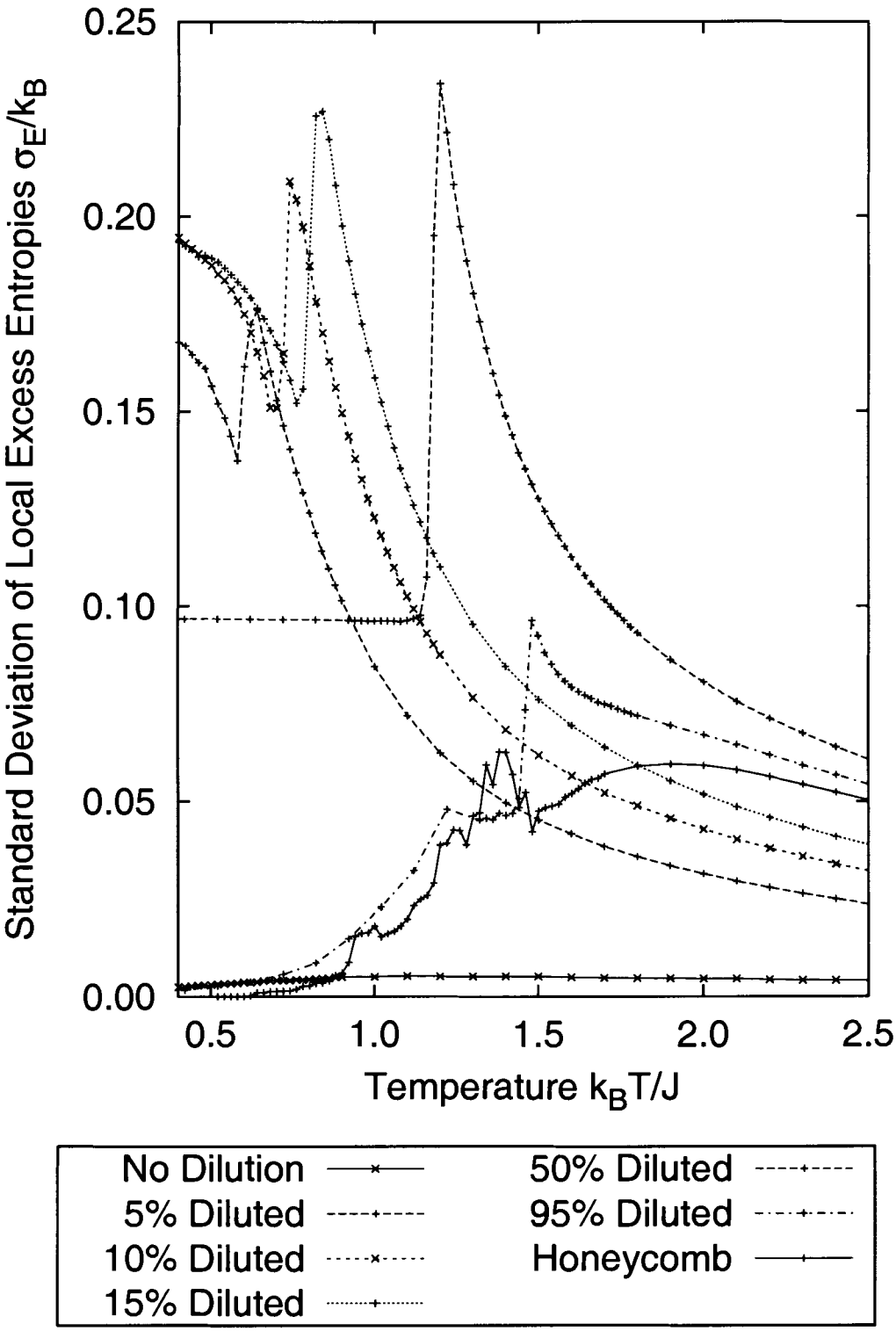

Figure 52: Standard deviation of excess entropy σ_E/k_B vs. temperature k_BT/J for a 98×99 lattice with 0 %, 5 %, 10 %, 15 %, 50 %, 95 %, and 100 % dilutions of sublattice A. Measurements were taken every $20\,MCS$ and there were $500,000$ measurements contributing to the average.

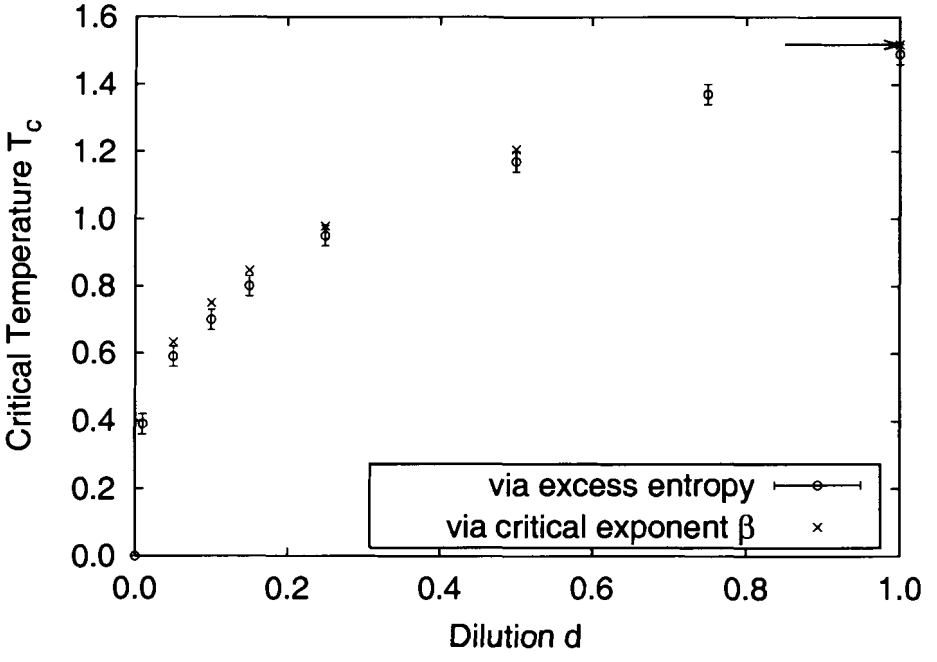

Figure 53: Critical temperature T_c vs. dilution d for the critical exponent method and the excess entropy method. Each run for the critical exponent method was done on a 98×99 lattice with an average over $30,000$ measurements.

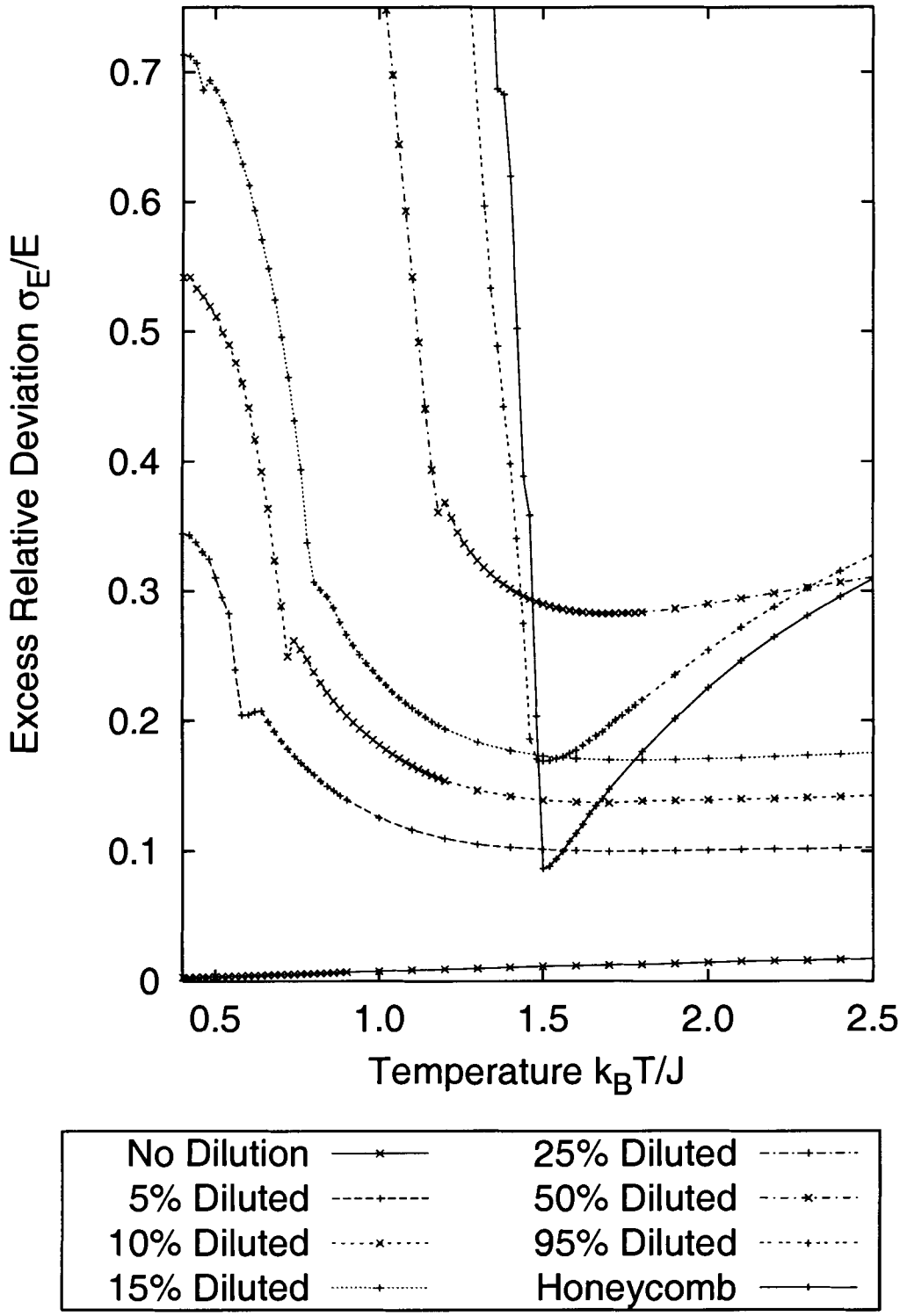

Figure 54: Relative deviation of excess entropy σ_E/E vs. temperature k_BT/J for various dilutions of sublattice A. Measurements were taken every 20 MCS on a 98×99 lattice and there were 500,000 measurements contributing to the average.

CHAPTER 6

CONCLUSIONS

In this investigation, we have studied the effects of dilution of one sublattice of the Ising antiferromagnet on a triangular lattice using Monte Carlo simulations. In addition to calculating the usual thermodynamic quantities, such as magnetization density, a variation of the Edwards-Anderson order parameter, specific heat, sublattice magnetizations, and the entropy density, we have computed the Shannon entropy density and the excess entropy. In order to calculate these information theoretic measures, we have introduced a new approach, using planted shapes. This method also provides a spatial map, which shows that the entropy and excess entropy are not shared equally across the lattice.

6.1 The information theoretic method

This investigation provides the first application, to our knowledge, of an information theoretic approach on a triangular lattice and on a system with quenched disorder. Our results show that the approach, implemented with planted shapes, works well for systems with randomness. The Shannon entropy rate $\Delta H(L)$ not only converges to the thermodynamic entropy for the undiluted, translationally invariant system as expected, but also converges in the case of random quenched dilution. The information theoretic technique of planting shapes yields a means of characterizing local contributions to the entropy density. This newly found way to quantify the ordering provides additional insight into the onset of the spin-glass phase.

The information theoretic method also provides the excess entropy, a measure of the system's complexity or information storage capacity. This quantity provides

a useful way to locate the critical temperature, which coincides with its peak in this system. Thus, this study provides evidence of the broader applicability of the information theoretic approach and its usefulness in characterizing phase transitions in systems with quenched disorder.

6.2 The model

Our results indicate that, even at very low dilutions, the system does undergo a phase transition. As dilution is increased, the residual entropy density falls faster than the linear approximation in the zero dilution limit, in agreement with the findings of Andérico, Fernández, and Streit (1982).

The local contributions to the entropy density show regions of great uncertainty near the quenched vacancies and are roughly uniform in the regions far from the vacancies. Below the critical temperature, they also show peaks associated with sites on the diluted sublattice (sublattice A). Some of the local contributions exhibit reentrance as a function of temperature, although the entropy density of the system decreases monotonically with temperature.

In the zero temperature limit, the local contributions to the entropy density show forbidden regions. For low dilutions, the forbidden regions are separated by thick bands and for moderate to high dilutions, the forbidden regions are separated by narrow bands. The spread, or standard deviation, of the local contributions increases as temperature decreases for systems with one sublattice diluted less than at least 95%. For systems with one sublattice diluted between $95 - 100\%$, the standard deviation of the local contributions as a function of temperature increases to a maximum and then drops. The relative deviation increases as temperature decreases for all non-zero dilutions.

The excess entropy of the diluted systems reaches a maximum at the critical temperature and the residual excess entropy, like the entropy density, is maximal

for zero dilution and monotonically decreases until it reaches zero in the honeycomb limit. The standard deviation of the local excess entropies grows as the temperature decreases, forms a cusp at its maximum value and then decreases as the temperature is lowered further.

6.3 Future work

The results of this investigation suggest several areas to be explored further, including:

- Analysis of the histograms to understand their explicit connections to the structure of the system;
- Determination of the information provided by the forbidden regions in the local entropy curves at low temperature;
- Exploration of the properties of the system in the vicinity of the critical sublattice dilution;
- Investigation of the effects of a magnetic field on the system, with the field applied either to all sites or only on one sublattice; and
- Extension of this model to a stacked, three-dimensional structure, to see how the behavior in three dimensions compares with that in two.

REFERENCES

Alexandrowicz, Z. (1971). Stochastic models for the statistical description of lattice systems. *Journal of Chemical Physics*, 55:2765–2779.

Alexandrowicz, Z. (1976). Entropy calculated from the frequency of states of individual particles. *Journal of Statistical Physics*, 14:1–9.

Andérico, C., Fernández, J., and Streit, T. (1982). Numerical study of the spin-glass transition in a dilute Ising model on a triangular lattice. *Physical Review B*, 26:3824–3830.

Bialek, W., Nemenman, I., and Tishby, N. (2001). Complexity through nonextensivity. *Physica A Statistical Mechanics and its Applications*, 302:89–99.

Bolzmann, L. (1877). On the Relation Between the Second Law of the Mechanical Theory of Heat and the Probability Calculus with Respect to the Theorems on Thermal Equilibrium. *Kais. Akad. Wiss. Wien Math. Naturwiss. Classe*, 76:373–435.

Choy, T. C. and Sherrington, D. (1983a). Antiferromagnetic triangular Ising model: An exact calculation of P(h). *Journal of Physics A Mathematical General*, 16:L265–L268.

Choy, T. C. and Sherrington, D. (1983b). CORRIGENDUM: Antiferromagnetic triangular Ising model: An exact calculation of P(h). *Journal of Physics A Mathematical General*, 16:3691.

Clausius, R. (1865). Über verschiedene für die Anwendung bequeme Formen der Hauptgleichung der mechanischen Wärmetheorie. *Annalen der Physik und Chimie*, 125:353–400.

Cover, T. and Thomas, J. (1991). *Elements of Information Theory.* John Wiley & Sons, Inc.

Crewick, R., Farach, H., Poole, C., and Knight, J. (1985). Monte Carlo study of the local-field distribution in the dilute antiferromagnetic Ising model on the triangular lattice. *Physical Review B*, 32:5776–5779.

Crutchfield, J. and Packard, N. (1983). Symbolic dynamics of noisy chaos. *Physica*, 7D:201–223.

Crutchfield, J. P. and Feldman, D. P. (2003). Regularities unseen, randomness observed: Levels of entropy convergence. *Chaos*, 13:25–54.

Domb, C. and Green, M. S. (1974). Phase transitions and critical phenomena. In Domb, C. and Green, M. S., editors, *Phase Transitions and Critical Phenomena.* Academic Press.

Edwards, S. F. and Anderson, P. W. (1975). Theory of spin glasses. *Journal of Physics F Metal Physics*, 5:965–974.

Eriksson, K. and Lindgren, K. (1989). Entropy and correlations in lattice systems. *Technical report, Physical Resource Theory Group, Chalmers University of Technology and University of Göteborg.*

Farach, H. A., Creswick, R. J., and Poole, C. P. (1988). Exact results for the site-dilute antiferromagnetic Ising model on finite triangular lattices. *Physical Review B*, 37:5615–5618.

Feldman, D. (1998). *Computational Mechanics of Classical Spin Systems.* PhD dissertation, University of California, Davis, Department of Physics.

Feldman, D. P. and Crutchfield, J. P. (1998). Measures of statistical complexity: Why? *Physics Letters A*, 238:244–252.

Feldman, D. P. and Crutchfield, J. P. (2003). Structural information in two-dimensional patterns: Entropy convergence and excess entropy. *Physical Review E, in press.*

Fernández, J. F., Andérico, C. Z., and Streit, T. S. J. (1982). Monte Carlo simulation of the spin-glass transition of a dilute Ising model on a triangular lattice. *Journal of Applied Physics*, 53:7991–7993.

Gibbs, W. (1902). *Elementary Principles in Statistical Mechanics.* Willard Gibbs.

Goldstein, S., Kuik, R., and Schlijper, A. G. (1990). Entropy and global Markov properties. *Comm. Math. Phys.*, 128:469–482.

Gonçalves, J. R., Poulter, J., and Blackman, J. A. (1997). Bond and site defects in fully frustrated two-dimensional Ising systems. *Journal of Physics A Mathematical General*, 30:2947–2962.

Grassberger, P. (1986). Towards a quantitative theory of self-generated complexity. *International Journal of Theoretical Physics*, 25(9):907–938.

Grest, G. S. and Gabl, E. G. (1979). Monte Carlo study of spin-glass ordering on dilute frustrated lattices. *Physical Review Letters*, 43:1182–1185.

Kaya, H. and Berker, N. A. (2000). Multiplicity of ordered phases in frustrated systems obtained from hard-spin mean-field theory. *Physical Review E*, 62:1469–1473.

Khinchin, A. I. (1957). *Information Theory.* Dover.

Lindgren, K. and Norhdal, M. (1988). Complexity measures and cellular automata. *Complex Systems*, 2:409–440.

Marčelja, S. (1996). Entropy of phase-separated structures. *Physica A Statistical Mechanics and its Applications*, 231:168–177.

Meirovitch, H. (1977). Calculation of entropy with computer simulation methods. *Chemical Physics Letters*, 45:389–392.

Meirovitch, H. (1983a). Computer simulation of self-avoiding walks: Testing the scanning method. *Journal of Chemical Physics*, 79:502–508.

Meirovitch, H. (1983b). Methods for estimating entropy with computer simulation: the simple cubic Ising lattice. *Journal of Physics A Mathematical General*, 16:839–847.

Meirovitch, H. (1984). Computer simulation study of hysteresis and free energy in the fcc Ising antiferromagnet. *Physical Review B*, 30:2866–2874.

Meirovitch, H. (1999). Simulation of a free energy upper bound, based on the anticorrelation between an approximate free energy functional and its fluctuation. *Journal of Chemical Physics*, 111:7215–7224.

Metropolis, N., Rosenbluth, A., Rosenbluth, M., Teller, A., and Teller, E. (1953). Equation of State Calculation by Fast Computing Machines. *Journal of Chemical Physics*, 21:1087.

Nemenman, I. M. (2000). *Information theory and learning: A physical approach.* PhD dissertation, Princeton University.

Netz, R. R. and Berker, A. N. (1991a). Hard-spin mean-field theory: Formulation for Ising, XY, and other models. *Journal of Applied Physics*, 70:6074–6076.

Netz, R. R. and Berker, A. N. (1991b). Monte Carlo mean-field theory and frustrated systems in two and three dimensions. *Physical Review Letters*, 66:377–380.

Newman, M. E. J. and Barkema, G. T. (1999). *Monte Carlo Methods in Statistical Physics.* Oxford University Press, Inc.

Olbrich, E., Hegger, R., and Kantz, H. (2000). Local estimates for entropy densities in coupled map lattices. *Physical Review Letters*, 84:2132–2135.

Planck, M. (1959). *The Theory of Heat Radiation.* Dover.

Reif, F. (1965). *Fundamentals of statistical and thermal physics.* McGraw Hill.

Schlijper, A. G. (1983). Convergence of the cluster-variation method in the thermodynamic limit. *Physical Review B*, 27:6841–6848.

Schlijper, A. G. and Smit, B. (1989). Two-sided bounds on the free energy from local states in Monte Carlo simulations. *Journal of Statistical Physics*, 56:247–260.

Schlijper, A. G., van Bergen, A. R. D., and Smit, B. (1990). Local-states method for the calculation of free energies in Monte Carlo simulations of lattice models. *Physical Review A*, 41:1175–1178.

Shannon, C. E. (1948). A mathematical theory of communication. *Bell System Tech. J.*, 27:379–423,623–656.

Shaw, R. (1984). *The Dripping Faucet as a Model Chaotic System.* Aerial Press.

Szépfalusy, P. and Györgyi, G. (1986). Entropy decay as a measure of stochasticity in chaotic systems. *Physical Review A*, 33:2852–2855.

Vink, R. L. and Barkema, G. T. (2002). Configurational Entropy of Network-Forming Materials. *Physical Review Letters*, 89:76405–76408.

Wannier, G. H. (1950). Antiferromagnetism. The triangular Ising net. *Physical Review*, 79:357–364.

APPENDIX

ORAL PRESENTATIONS

- March 6, 2003 *American Physical Society Annual March Meeting* "Local Ordering and Structure in the Ising Antiferromagnet on a Triangular Lattice with Quenched Dilution"
  http://www.aps.org/meet/MAR03/baps/abs/S7910004.html

- October 19, 2002 *Greater Boston Area Statistical Mechanics Meeting* "An Information Theoretic Study of the Ising Antiferromagnet on a Triangular Lattice with Quenched Vacancies"
  http://physics.clarku.edu/gbasm/fall2002/#session2

- March 20, 2002 *American Physical Society Annual Meeting* "A Detailed Look at the Entropy and Excess Entropy in a Transition where Order Arises from Quenched Disorder"
  http://www.aps.org/meet/MAR02/baps/abs/S4200010.html

BIOGRAPHY OF THE AUTHOR

Matthew David Robinson was born in Reno, Nevada on June 9, 1974. He graduated from Churchill County High School in 1992. Matt began his undergraduate career at the University of Nevada, Las Vegas and after three semesters transferred to the University of Nevada, Reno. After six years in Reno, Matt was awarded a Bachelors of Science degree in the two major programs of Applied Mathematics and Physics as well as a Bachelors of Arts degree in the major area of Philosophy. He began his graduate work there and in the Fall of 2000 was accepted as a graduate student in the Department of Physics and Astronomy at The University of Maine.

Matt is a candidate for a Master of Science degree in Physics from The University of Maine in August, 2003.